Constraining the mass-spectra in the presence of a light sterile neutrino from absolute mass-related observables

Srubabati Goswami[,1,2,*] Debashis Pachhar[,1,3,†] and Supriya Pan[1,‡]

[1]*Physical Research Laboratory, Ahmedabad, Gujarat 380009, India*
[2]*Northwestern University, Department of Physics and Astronomy, Evanston, Illinois 60208, USA*
[3]*Indian Institute of Technology Gandhinagar, Gujarat 382355, India*

The framework of three-flavor neutrino oscillation is a well-established phenomenon, but results from the short-baseline experiments, such as the Liquid Scintillator Neutrino Detector (LSND) and MiniBooster Neutrino Experiment (MiniBooNE), hint at the potential existence of an additional light neutrino state characterized by a mass-squared difference of approximately 1 eV^2. The new neutrino state is devoid of all Standard Model (SM) interactions, commonly referred to as a "sterile" state. In addition, a sterile neutrino with a mass-squared difference of 10^{-2} eV^2 has been proposed to improve the tension between the results obtained from the Tokai to Kamioka (T2K) and the NuMI Off-axis ν_e Appearance (NOνA) experiments. Further, the nonobservation of the predicted upturn in the solar neutrino spectra below 8 MeV can be explained by postulating an extra light sterile neutrino state with a mass-squared difference around 10^{-5} eV^2. The hypothesis of an additional light sterile neutrino state introduces four distinct mass spectra depending on the sign of the mass-squared difference. In this paper, we discuss the implications of the above scenarios on the observables that depend on the absolute mass of the neutrinos; namely, the sum of the light neutrino masses (Σ) from cosmology, the effective mass of the electron neutrino from beta decay (m_β), and the effective Majorana mass ($m_{\beta\beta}$) from neutrinoless double beta decay. We show that some scenarios can be disfavored by the current constraints of the above variables. The implications for projected sensitivity of Karlsruhe Tritium Neutrino Experiment (KATRIN) and future experiments like Project-8, next Enriched Xenon Observatory (nEXO) are discussed.

DOI: 10.1103/PhysRevD.110.015028

I. INTRODUCTION

The phenomena of neutrino oscillations, in which neutrino flavor states switch their identities while propagating, have been observed in several terrestrial experiments [1–4]. This requires at least two of the neutrinos to have small but nonzero masses and mixing between the different flavors. This, in turn, implies physics beyond the Standard Model (BSM). Many BSM scenarios have been studied for generating neutrino masses. The smallness of the neutrino masses is often linked with lepton number violation through the dimension 5 Weinberg operator $\frac{LLHH}{\Lambda}$ [5]. This operator violates the lepton number, which signifies the Majorana nature of the neutrinos.

*sruba@prl.res.in
†debashispachhar@prl.res.in
‡supriyapan@prl.res.in

Neutrino oscillation experiments are sensitive to two mass-squared differences and mixing angles of the neutrinos. However, they cannot shed light on the absolute mass scale or the nature of neutrinos. If neutrinos are considered to be Majorana in nature, a rare and slow nuclear decay, known as neutrinoless double beta decay ($0\nu\beta\beta$) [6], can exist in nature. Several experiments aimed to observe this process, but there has not been any positive evidence so far. The KamLAND-Zen experiment using the Xe^{136} isotope as the decaying nucleus gives the lower bound on the half-live as $T_{1/2}^{0\nu\beta\beta} > 1.07 \times 10^{26}$ yr at 90% confidence level [7] whereas the GERDA experiment uses Ge^{76} isotope and their latest limit on the half-life is $T_{1/2}^{0\nu\beta\beta} > 1.8 \times 10^{26}$ yr at 90% confidence level [8]. The lower bounds on half-lives can be translated into upper bounds on the effective Majorana mass parameter ($m_{\beta\beta}$), which depends on the neutrino masses, mixing angles, and the Majorana phases.

The information about the absolute mass scale of neutrinos can also come from tritium beta decay. The KATRIN experiment sets the current limit on the mass parameter, $m_\beta \lesssim 0.8$ eV at 90% confidence level [9].

Cosmological observations like CMB anisotropies, large-scale structure formation, etc., can also put bound on the absolute mass scale of neutrinos. The most stringent bound on the sum of the light neutrino masses (Σ) < 0.12 eV comes from the Planck Collaboration by considering three degenerate neutrino mass eigenstates [10].

Although the three-generation paradigm is well established, there are experimental anomalies that indicate the presence of an extra light sterile neutrino of mass of the order of eV. The short baseline experiments, LSND [11] and MiniBooNE [12], showed an excess signature of electron neutrinos coming from a muon neutrino beam. Gallium-based solar neutrino experiments GALLEX [13], SAGE [14], and as well as the BEST [15] experiments found the deficit in electron neutrinos while calibrating the detector using the neutrinos from ^{51}Cr and ^{37}Ar sources. One possible resolution of the results from these experiments is provided by incorporating an additional light neutrino state with mass $\sim$1 eV [16]. The MiniBooNE experiment also reported a low-energy excess in the electron events above the background. MicroBooNE detector was designed to test this excess using a liquid argon time projection chamber detector with superior particle identification and background rejection capability. The first MicroBooNE results did not report this excess in the electron events in their three years of data [17–19] and the results are consistent with the 3ν hypothesis within 1σ significance [20]. However, in Ref. [21], it was shown that the electron disappearance data from MicroBooNE indicates oscillations with the highest significance of 2.4σ (using the Feldman-Cousins approach) coming from the Wire-Cell analysis. The preferred parameters are quoted as $\sin^2(2\theta_{14}) = 0.35^{+0.19}_{-0.16}$ and $\Delta m^2_{41}(\equiv \Delta m^2_s) = 1.25^{+0.74}_{-0.39}$ eV^2. Moreover, the joint analysis of the results from MiniBooNE and MicroBooNE experiments preferred the $3 + 1$ scenario over no oscillation [22].

There are also motivations for considering sterile neutrinos lower than the eV scale. The inclusion of a sterile neutrino with mass squared difference $(\Delta m^2_s) \sim 10^{-5}$ eV^2 has been postulated to explain the absence of the upturn of solar neutrino probability below 8 MeV [23]. Additionally, it is also shown that the tension between NOνA and T2K data can be reduced in the presence of a sterile neutrino with $\Delta m^2_s \sim (10^{-4}: 10^{-2})$ eV^2 [24]. Recently, the signatures of the sub-eV sterile neutrinos in future experiments have been studied in Refs. [25–28] in the context of future long-baseline atmospheric neutrino experiments.

In this paper, we study the implication of a very light sterile neutrino with Δm^2_s in the range $(10^{-4}: 10^{-2})$ eV^2 on the mass-related variables such as $m_{\beta\beta}, m_\beta$, and Σ. Such investigations in the context of an eV scale sterile neutrino have been explored in [29]. In our work, along with the sub-eV scale sterile neutrino we also present the results for an eV scale sterile neutrino with the current constraints on

the mixing the parameters. We consider the $3 + 1$ picture with a single sterile neutrino added to the three sequential neutrinos. In this case, there can be four mass possible spectra; two each with $\Delta m^2_s > 0$ and $\Delta m^2_s < 0$. We explore the implication of the cosmological constraint on the sum of light neutrino masses for these spectra. We also discuss the constraints on the possible mass spectra in the light of KATRIN results on m_β and KamLAND-Zen results on $m_{\beta\beta}$. Additionally, we examine the implications of the future measurements by proposed experiments Project8, nEXO [30,31].

The outline of the paper is as follows. Section II gives a brief overview of the neutrino mass and mixing scenarios in the standard three-generation and $3 + 1$ framework. In Sec. III, we study the implications of the various mass spectra for $\Sigma, m_{\beta\beta}$, and m_β. Section IV presents an analysis on the correlation between $m_{\beta\beta}, m_\beta$, and Σ. Finally, we summarize the results in Sec. V.

II. NEUTRINO MASSES AND MIXING

A. The standard framework

Neutrino oscillation is governed by the Pontecorvo-Maki-Nakagawa-Sakata (PMNS) matrix (U), which describes the relationship between the neutrino flavor and mass eigenstates [32]. The mass matrix in the flavor basis $\mathcal{M}_\nu$ and the mass matrix in the mass basis M^{diag}_ν are related as

$$\mathcal{M}_\nu = U M^{\text{diag}}_\nu U^T, \tag{1}$$

$$\text{where } M^{\text{diag}}_\nu = \text{diag}(m_1, m_2, m_3). \tag{2}$$

The PMNS matrix is parametrized by three mixing angles $(\theta_{12}, \theta_{13}, \theta_{23})$ and one CP Phase (δ_{13}) for Dirac neutrinos, whereas Majorana nature of neutrino adds two extra phases (α, β) along with it. Various oscillation experiments provide information about the mixing angles $(\theta_{12}, \theta_{13}, \theta_{23})$ and mass-squared differences $(\Delta m^2_{\text{sol}}, \Delta m^2_{\text{atm}})$. Here $\Delta m^2_{\text{sol}} > 0$ and defined as $m^2_2 - m^2_1$. Depending on the sign of Δm^2_{atm}, the masses in the three-flavor framework are categorized into two mass orderings:

(i) Normal ordering (NO): In NO, $\Delta m^2_{\text{atm}} \equiv m^2_3 - m^2_1 > 0$. The mass ordering in this scenario is $m_1 < m_2 < m_3$, and the mass relations can be expressed as

$$m_{\text{lightest}} = m_1, \qquad m_2 = \sqrt{m^2_1 + \Delta m^2_{\text{sol}}},$$
$$m_3 = \sqrt{m^2_1 + \Delta m^2_{\text{atm}}}. \tag{3}$$

(ii) Inverted ordering (IO): In this case, the mass ordering is $m_3 < m_1 < m_2$ and $\Delta m^2_{\text{atm}} \equiv m^2_3 - m^2_2 < 0$.

TABLE I. 3σ ranges and best fit values extracted of three neutrino oscillation parameters [33]. Here, $\Delta m^2_{\text{sol}} \equiv m^2_2 - m^2_1$ and $\Delta m^2_{\text{atm}} \equiv m^2_3 - m^2_1$ for NO and $m^2_2 - m^2_3$ for IO.

Parameters	Normal ordering		Inverted ordering	
	3σ range	Best fit	3σ range	Best fit
$\sin^2 \theta_{12}$	0.270:0.341	0.303	0.270:0.341	0.303
θ_{12}	31.31°:35.74°	33.41°	31.31°:35.74°	33.41°
$\sin^2 \theta_{13}$	0.0202:0.0239	0.0220	0.0202:0.0239	0.0220
θ_{13}	8.19°–8.89°	8.54°	8.23°:8.90°	8.57°
$\sin^2 \theta_{23}$	0.406:0.620	0.572	0.412:0.623	0.578
θ_{23}	39.6°:51.9°	49.1°	39.9°:52.1°	49.5°
δ_{13}	197°	108°:404°	286°	192°:360°
$\Delta m^2_{\text{sol}}/10^{-5}$ eV^2	6.82:8.03	7.41	6.82:8.03	7.41
$\Delta m^2_{\text{atm}}/10^{-3}$ eV^2	2.428:2.597	2.511	$(-2.581:-2.408)$	-2.498

In this ordering, the mass relation ns are written as

$$m_{\text{lightest}} = m_3, \qquad m_2 = \sqrt{m_3^2 + \Delta m^2_{\text{atm}}},$$

$$m_1 = \sqrt{m_3^2 + \Delta m^2_{\text{atm}} - \Delta m^2_{\text{sol}}}. \qquad (4)$$

(iii) Quasidegenerate spectrum (QD): Apart from NO and IO, there might be a scenario where $m_1 \approx m_2 \approx m_3$. This scenario is generally referred to as quasidegenerate spectrum. In this scenario, the value of the lightest mass is greater than $\sqrt{\Delta m^2_{\text{atm}}}$.

The current best-fit and 3σ range of these parameters, determined from various experiments, are given in Table I.

B. The 3 + 1 framework

In this case, we have one extra mass-squared difference ($\Delta m^2_s \equiv m^2_4 - m^2_1$), three new mixing angles ($\theta_{14}, \theta_{24}\theta_{34}$) and two new Dirac CP phases (δ_{14}, δ_{24}) and one additional Majorana phase (γ). The mass matrix in the flavor basis can be defined as

$$\mathcal{M}^s_\nu = U M^{\text{diag}}_\nu U^T, \quad \text{where } M^{\text{diag}}_\nu = \text{diag}(\mathrm{m}_1, \mathrm{m}_2, \mathrm{m}_3, \mathrm{m}_4). \qquad (5)$$

In the 3 + 1 framework, the mixing matrix U can be parametrized as

$$U = R_{34}(\theta_{34})\tilde{R}_{24}(\theta_{24}, \delta_{24})\tilde{R}_{14}(\theta_{14}, \theta_{14})R_{23}(\theta_{23})$$
$$\times \tilde{R}_{13}(\theta_{13}, \delta_{13})R_{12}(\theta_{12})P$$
$$= \begin{pmatrix} U_{e1} & U_{e2} & U_{e3} & U_{e4} \\ U_{\mu1} & U_{\mu2} & U_{\mu3} & U_{\mu4} \\ U_{\tau1} & U_{\tau2} & U_{\tau3} & U_{\tau4} \\ U_{s1} & U_{s2} & U_{s3} & U_{s4} \end{pmatrix}, \qquad (6)$$

where R_{ij}'s are the standard rotational matrices in the i, j generational space. For instance,

$$R_{34}(\theta_{34}) = \begin{pmatrix} 1 & 0 & 0 & 0 \\ 0 & 1 & 0 & 0 \\ 0 & 0 & c_{34} & s_{34} \\ 0 & 0 & -s_{34} & c_{34} \end{pmatrix},$$

$$\tilde{R}_{14}(\theta_{14}, \delta_{14}) = \begin{pmatrix} c_{14} & 0 & 0 & s_{14}e^{-i\delta_{14}} \\ 0 & 1 & 0 & 0 \\ 0 & 0 & 1 & 0 \\ -s_{14}e^{i\delta_{14}} & 0 & 0 & c_{14} \end{pmatrix}. \qquad (7)$$

Here, $c_{ij}(s_{ij})$ stands for $\cos\theta_{ij}(\sin\theta_{ij})$ and P is the diagonal matrix containing the Majorana phases, defined as $P = \text{diag}(1, e^{i\frac{\alpha}{2}}, e^{i(\frac{\beta}{2}+\delta_{13})}, e^{i(\frac{\gamma}{2}+\delta_{14})})$. In Table II, we present three representative values of Δm^2_s and $\sin^2\theta_{14}$ extracted from the allowed region from MINOS, MINOS$^+$, Daya-Bay, and Bugey-3 experiments [34,35]. The value of $\sin^2\theta_{14}$ analyzing the LSND and MiniBooNE data is in the range $(0.01:0.02)$ for $\Delta m^2_s = 1.3$ eV^2, whereas the MINOS and MINOS$^+$ data allows the region with $\sin^2\theta_{14}$ is <0.01.

TABLE II.   Allowed values of the sterile neutrino parameters $\Delta m^2_s, \sin^2\theta_{14}$ in the 3 + 1 scenario for three different mass-squared differences ($\Delta m^2_s = 10^{-4}$ eV^2, 0.01 eV^2, and 1.3 eV^2) are given. The value of the $\sin^2\theta_{14}$ is chosen to be consistent with MINOS, MINOS$^+$, Daya-Bay, and Bugey-3 data [34].

Parameters	Case I	Case II	Case III
Δm^2_s	10^{-4} eV^2	10^{-2} eV^2	1.3 eV^2
$\sin^2\theta_{14}$	0.1:0.2	$5 \times 10^{-4} : 5 \times 10^{-3}$	0.001:0.01
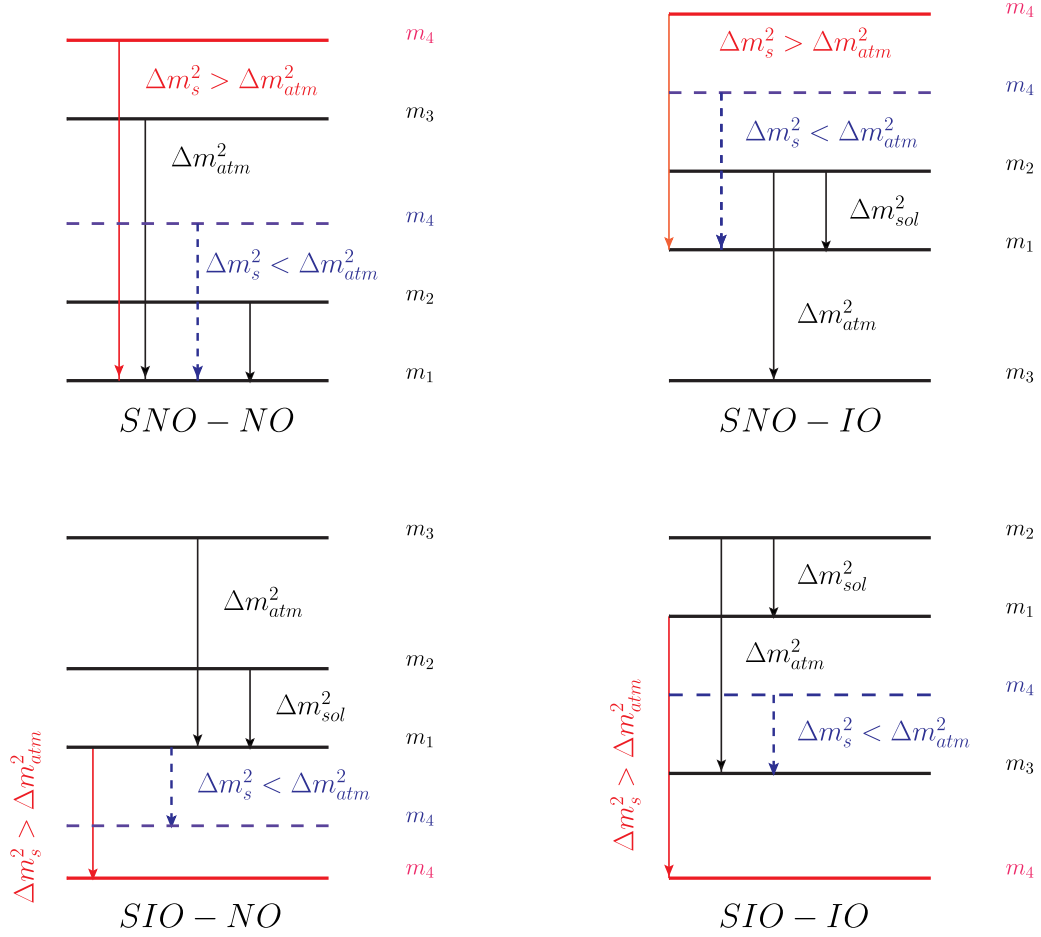
FIG. 1. Possible mass spectra with the inclusion of a sterile neutrino. Here red solid line corresponds to the value of m_4 when $\Delta m_s^2 > \Delta m_{atm}^2$ whereas the blue dashed line indicates the same with $\Delta m_s^2 < \Delta m_{atm}^2$.

In the $3 + 1$ framework, the sign and the magnitude of Δm_s^2 lead to different mass spectra:

(1) SNO-NO ($\Delta m_s^2 > 0, \Delta m_{atm}^2 > 0$)

In this scenario, mass ordering is different for $\Delta m_s^2 > \Delta m_{atm}^2$ and $\Delta m_s^2 < \Delta m_{atm}^2$ which is depicted in the top left corner of Fig. 1 with a red solid line and a blue dashed line, respectively. For $\Delta m_s^2 > \Delta m_{atm}^2$, the mass ordering is $m_1 < m_2 < m_3 < m_4$, given in the top left corner of Fig. 1. Whereas for $\Delta m_s^2 < \Delta m_{atm}^2$, the ordering is $m_1 < m_2 < m_4 < m_3$. In both cases, the mass relations are expressed as

$$m_{\text{lightest}} = m_1, \qquad m_2 = \sqrt{m_1^2 + \Delta m_{\text{sol}}^2},$$
$$m_3 = \sqrt{m_1^2 + \Delta m_{\text{atm}}^2}, \qquad m_4 = \sqrt{m_1^2 + \Delta m_s^2}. \tag{8}$$

(2) SNO-IO ($\Delta m_s^2 > 0, \Delta m_{\text{atm}}^2 < 0$)

In this case, the mass ordering is the same for both $\Delta m_s^2 > \Delta m_{\text{atm}}^2$ and $\Delta m_s^2 < \Delta m_{\text{atm}}^2$ and is delineated as $m_3 < m_1 < m_2 < m_4$. The mass relations are expressed as

$$m_{\text{lightest}} = m_3, \qquad m_2 = \sqrt{m_3^2 + \Delta m_{\text{atm}}^2},$$
$$m_1 = \sqrt{m_3^2 + \Delta m_{\text{atm}}^2 + \Delta m_{\text{sol}}^2}, \qquad m_4 = \sqrt{m_3^2 + \Delta m_{\text{atm}}^2 - \Delta m_{\text{sol}}^2 + \Delta m_s^2}. \tag{9}$$

(3) SIO-NO ($\Delta m_s^2 < 0, \Delta m_{\text{atm}}^2 > 0$)

The mass ordering in this scenario is defined as $m_4 < m_1 < m_2 < m_3$, and it is the same for both the Δm_s^2 ranges. The mass relations can be written as

$$m_{\text{lightest}} = m_4, \qquad m_2 = \sqrt{m_4^2 + \Delta m_s^2 + \Delta m_{\text{sol}}^2},$$
$$m_1 = \sqrt{m_4^2 + \Delta m_s^2}, \qquad m_3 = \sqrt{m_4^2 + \Delta m_s^2 + \Delta m_{\text{atm}}^2}. \tag{10}$$

(4) SIO-IO ($\Delta m_s^2 < 0, \Delta m_{\text{atm}}^2 < 0$)

(a) For $\Delta m_s^2 > \Delta m_{\text{atm}}^2$, the mass ordering is $m_4 < m_3 < m_1 < m_2$ and the mass relations are defined as

$$m_{\text{lightest}} = m_4, \qquad m_2 = \sqrt{m_4^2 + \Delta m_s^2 + \Delta m_{\text{sol}}^2},$$
$$m_1 = \sqrt{m_4^2 + \Delta m_s^2}, \qquad m_3 = \sqrt{m_4^2 + \Delta m_s^2 + \Delta m_{\text{sol}}^2 - \Delta m_{\text{atm}}^2}. \tag{11}$$

(b) For $\Delta m_s^2 < \Delta m_{\text{atm}}^2$, the mass ordering is $m_3 < m_4 < m_1 < m_2$ and the mass relations can be expressed as

$$m_{\text{lightest}} = m_3, \qquad m_2 = \sqrt{m_3^2 + \Delta m_{\text{atm}}^2},$$
$$m_1 = \sqrt{m_3^2 + \Delta m_{\text{atm}}^2 - \Delta m_{\text{sol}}^2}, \qquad m_4 = \sqrt{m_3^2 + \Delta m_{\text{atm}}^2 - \Delta m_{\text{sol}}^2 - \Delta m_s^2}. \tag{12}$$

In the Appendix, we have given the variation of masses (m_i) with respect to the lightest mass for all the scenarios.

III. NEUTRINO MASS VARIABLES

In this section, we study the implications of adding an additional sterile neutrino for the mass variables $m_{\beta\beta}, m_\beta, \Sigma$.

A. Bound from cosmology

Light sterile neutrinos can have a significant impact on the evolution of the Universe, and thus, their presence can be investigated using cosmological observations. If sterile neutrinos are massless, they contribute to the light relativistic degrees of freedom in the early Universe, quantified as N_{eff}, which can be directly constrained from cosmic microwave background (CMB) and large-scale structure (LSS) data. The Standard Model of particle physics predicts $N_{\text{eff}}^{\text{SM}} = 3.044_{-0.0002}^{+0.0002}$ [36–38], assuming only three degenerate light active neutrinos, but can increase in general when the sterile neutrino contribution is added.[1]

In the case of massive sterile neutrinos, one needs to add one more free parameter, m_s^{eff}, the effective sterile neutrino mass in the cosmological models along with N_{eff}. The effective sterile neutrino mass is different from its physical mass (m_s^{ph}) but can be related as $m_s^{\text{eff}} = \Delta N_{\text{eff}}^{3/4} m_s^{\text{ph}}$ if the neutrinos are fully thermalized with active neutrinos and

$m_s^{\text{eff}} = \Delta N_{\text{eff}} m_s^{\text{ph}}$ for the partially thermalized sterile neutrinos where $\Delta N_{\text{eff}} = N_{\text{eff}} - N_{\text{eff}}^{\text{SM}}$.

When PLANK 2018 data is fitted with standard Λ_{CDM} cosmological model, it tends to disfavor the presence of extra light relativistic degrees of freedom [10]. However, with the inclusion of more parameters with the standard Λ_{CDM} cosmological model and fitting more data from different cosmological observations, the cosmological constraints can be relaxed. For example, in a recent analysis, the Plank + BAO + Hubble parameter measurement [43] + Supernova Ia [44] data fitted with a 10 parameter cosmological model (10-PCM) i.e., $\Lambda_{\text{CDM}} + N_{\text{eff}} + m_{\text{eff}}^s + w_0 + n_{run}$, gives the constraints on N_{eff} and Σ as follows [35]:

$$N_{\text{eff}} = 3.11_{-0.36}^{+0.37}, \qquad \Sigma = 0.16 \text{ eV}, \tag{13}$$

where ω_0 is the equation of state parameter of the dark energy and n_{run} is the running of the scalar spectral index, a parameter related to the initial conditions of the universe. Another model with 12 parameters, called extended Λ_{CDM} ($e\Lambda_{\text{CDM}}$) gives bound as

$$N_{\text{eff}} = 3.11_{-0.48}^{+0.52}, \qquad \Sigma = 0.52 \text{ eV}, \tag{14}$$

where Σ is defined as [45]

$$\Sigma = m_1 + m_2 + m_3 + m_s^{\text{eff}}. \tag{15}$$

---

[1]However, N_{eff} can be decreased in certain scenarios like very low-reheating in sterile neutrinos [39,40] or self-interacting sterile neutrinos [41,42].
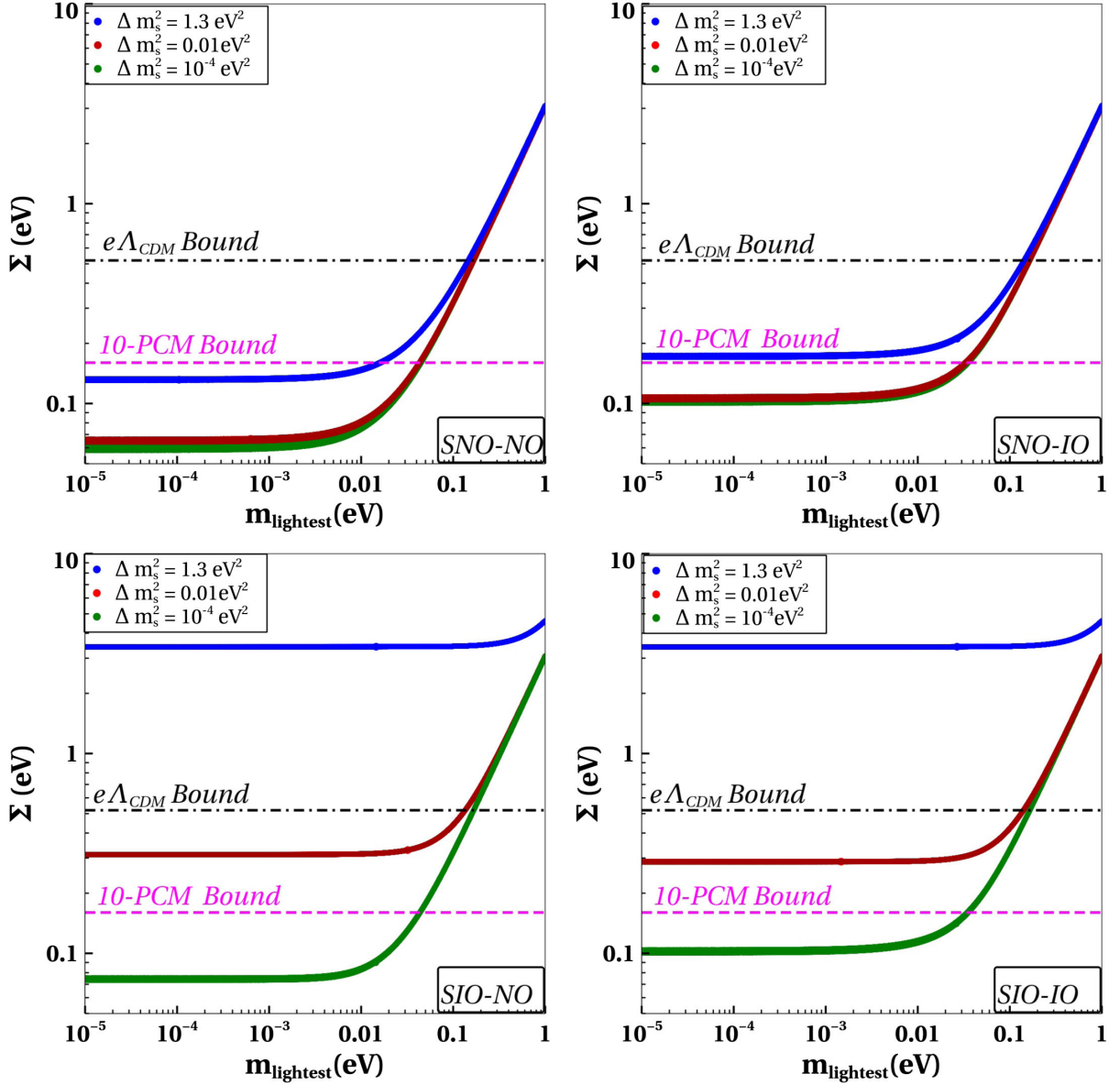
FIG. 2. The variation total effective mass Σ with the lightest neutrino mass m_{lightest} in different scenarios SNO-NO (top left), SNO-IO (top right), SIO-NO (bottom left), and SIO-IO (bottom right). The green, red, and blue colors correspond to $\Delta m_s^2 = 10^{-4}$ eV^2, 0.01 eV^2, 1.3 eV^2, respectively. The magenta dashed line corresponds to the 10-PCM and the black dashed-dot line corresponds to the extended Λ_{CDM} ($e\Lambda_{\text{CDM}}$) bound.

A fully thermalized neutrino implies $\Delta N_{\text{eff}} \approx 1$, which is ruled out from the cosmological data [35]. However, there are interesting ideas to tamper with the sterile neutrino thermalization and maintain N_{eff} around $N_{\text{eff}}^{\text{SM}}$. These ideas include large chemical potentials [46–49], secret interactions of the sterile neutrinos [41,50–53], and a low reheating temperature of the universe [39,54–56]. Recently, an interesting scenario was proposed where a cosmologically viable eV scale sterile neutrino is produced from an ultralight pseudoscalar which can also be a possible candidate for dark matter [57]. The sterile neutrino is produced nonthermally which means $m_s^{\text{eff}} = \Delta N_{\text{eff}} m_4$, where m_4 is the physical mass of the sterile neutrino.

We have plotted Σ as a function of the lightest neutrino mass for different mass schemes in Fig. 2 assuming the value of $N_{\text{eff}} = 3.11$ from Eqs. (13) and (14). The pink dashed line indicates the limit $\Sigma = 0.16$ eV, and the black dashed-dot line corresponds to $\Sigma = 0.52$ eV.

The important features observed from Fig. 2 are as follows:

(i) The SNO-NO scenario is favored by $e\Lambda_{\text{CDM}}$ model up to $m_{\text{lightest}} \sim 0.15$ eV for all the three mass-squared differences. Whereas the 10-PCM is more constraining and disfavor $\Delta m_s^2 = 1.3$ eV^2 above $m_{\text{lightest}} > 0.01$ eV and $\Delta m_s^2 = 10^{-4}$ eV^2, 0.01 eV^2 above $m_{\text{lightest}} > 0.04$ eV.

TABLE III. The table summarises the status of four mass spectra for three different Δm_s^2 in the light of different cosmological models. The limits correspond to the value of m_{lightest} up to which the scenario is allowed.

Mass ordering (m_{lightest})	$\Delta m_s^2 = 10^{-4}$ eV^2		$\Delta m_s^2 = 0.01$ eV^2		$\Delta m_s^2 = 1.3$ eV^2	
	Limit 10 − PCM	Limit eΛ_{CDM}	Limit 10 − PCM	Limit $e\Lambda_{\text{CDM}}$	Limit 10 − PCM	Limit eΛ_{CDM}
SNO-NO (m_1)	<0.04	<0.15	<0.04	<0.15	<0.01	<0.15
SNO-IO (m_3)	<0.03	<0.1	<0.03	<0.1	Disallowed	<0.1
SIO-NO (m_4)	<0.04	<0.1	Disallowed	<0.1	Disallowed	Disallowed
SIO-IO (m_3/m_4)	<0.04	<0.1	Disallowed	<0.1	Disallowed	Disallowed

(ii) For SNO-IO, $e\Lambda_{\text{CDM}}$ model allows all values of Δm_s^2 up to $m_{\text{lightest}} \sim 0.15$ eV. However, $\Delta m_s^2 = 1.3$ eV^2 is disfavored by the 10-PCM for the entire range of m_{lightest}. The lower values of Δm_s^2 are still allowed up to $m_{\text{lightest}} \sim 0.04$ eV.

(iii) For SIO-NO and SIO-IO, the 10-PCM disfavors $\Delta m_s^2 = 0.01$ eV^2 and 1.3 eV^2 for the entire range of m_{lightest} but $\Delta m_s^2 = 10^{-4}$ eV^2 is still allowed up to $m_{\text{lightest}} \sim 0.03$ eV. However, if we consider $e\Lambda_{\text{CDM}}$ model, then $\Delta m_s^2 = 0.01$ eV^2 gets allowed up to $m_{\text{lightest}} \sim 0.1$ eV.

The above discussion is summarized in Table III.

B. Bound from tritium β decay

A direct and model-independent constraint on the neutrino mass can be derived through the experimental analysis of the electron energy spectrum resulting from beta decay in atomic nuclei. In beta decay, the energy excess due to the nuclear mass difference is shared among the electron, (anti)neutrino and the daughter nucleus. If the energy resolution of the experiment exceeds the splittings of the neutrino mass states ($\Delta E \gg m_i$) then the emitted electron's spectrum depends on a quantity called the "kinematic mass" of the electron neutrino which is defined as

$$
\begin{aligned}
m_\beta &= \sqrt{|U_{e1}|^2 m_1^2 + |U_{e2}|^2 m_2^2 + |U_{e3}|^2 m_3^2 + |U_{e4}|^2 m_4^2} \\
&= \sqrt{c_{12}^2 c_{13}^2 c_{14}^2 m_1^2 + s_{12}^2 c_{13}^2 c_{14}^2 m_2^2 + s_{13}^2 c_{14}^2 m_3^2 + s_{14}^2 m_4^2}.
\end{aligned} \tag{16}
$$

The kinematic mass depends on the mixing parameters, mass squared differences, and the lightest neutrino mass. The current KATRIN limit on m_β is ≤ 0.8 eV and the future sensitivity is quoted as $m_\beta \leq 0.2$ eV. We have plotted m_β as a function of the lightest neutrino mass in Fig. 3 by varying all the parameters in their respective allowed intervals as given in Table II. The cyan dashed lines in the figure show the projected sensitivity of the KATRIN experiment of 0.2 eV. In this figure, we also show the sensitivity of future experiment Project 8 [30], by a dashed-dot black line, which plans to probe the lightest neutrino mass with a maximum sensitivity of up to 40 meV in a phased manner. In Fig. 3, $|U_{e1}|^2, |U_{e2}|^2, |U_{e3}|^2$ are varied $(0.64{:}0.72)$, $(0.26{:}0.33), (0.020{:}0.024)$ and the range of $|U_{e4}|^2$ as given in Table II. In Table IV, we provide the necessary values to explain the characteristics of Fig. 3.

The following observations can be made from Fig. 3:

(1) KATRIN's future sensitivity allows us to probe m_β only above $m_{\text{lightest}} \sim 0.2$ eV for SNO-NO, SNO-IO for all values of Δm_s^2. In case of SIO-NO, SIO-IO KATRIN will be able to probe the entire spectrum of m_{lightest} for $\Delta m_s^2 = 1.3$ eV^2, and above $m_{\text{lightest}} \sim 0.02$ eV for $\Delta m_s^2 = 10^{-4}$ eV^2, 0.01 eV^2.

(2) The sensitivity of Project 8 allows us to probe m_β only above $m_{\text{lightest}} \sim 0.03$ eV for SNO-NO and SIO-NO of $\Delta m_s^2 = 10^{-4}$ eV^2. However, Project 8 experiment can probe SNO-IO, SIO-NO, and SIO-IO for $\Delta m_s^2 = 0.01$ eV^2 and 1.3 eV^2 in the entire range of m_{lightest}.

(3) SNO-NO: Using Eq. (8), m_β can be approximated as

$$
m_\beta^{\text{SNO−NO}} = \sqrt{m_{\text{lightest}}^2 + |U_{e2}|^2 \Delta m_{\text{sol}}^2 + |U_{e3}|^2 \Delta m_{\text{atm}}^2 + |U_{e4}|^2 \Delta m_s^2}. \tag{17}
$$

(a) For $m_{\text{lightest}} < \sqrt{\Delta m_{\text{sol}}^2} < \sqrt{\Delta m_{\text{atm}}^2}$, it is seen from Table IV that the second, third and the fourth term in Eq. (17) varies in the similar range for $\Delta m_s^2 = 10^{-4}$ eV^2 and $\Delta m_s^2 = 0.01$ eV^2. Hence $m_\beta^{\text{SNO−NO}}$ varies as $(0.009{:}0.01)$ and $(0.008{:}0.011)$ eV. In the case of $\Delta m_s^2 = 1.3$ eV^2, $m_\beta^{\text{SNO−NO}} \approx |U_{e4}|\sqrt{\Delta m_s^2}$ and varies between $(0.036{:}0.114)$ eV.

(b) For $\sqrt{\Delta m_{\text{sol}}^2} < m_{\text{lightest}} < \sqrt{\Delta m_{\text{atm}}^2} < \sqrt{\Delta m_s^2}$, $m_{\beta\beta}^{\text{SNO−NO}} \approx m_{\text{lightest}}$ for $\Delta m_s^2 = 10^{-4}$ eV^2 and $\Delta m_s^2 = 0.01$ eV^2, whereas $|U_{e4}|^2 \Delta m_s^2$ still dominates in this region for $\Delta m_s^2 = 1.3$ eV^2.

(c) For $\sqrt{\Delta m_{\text{atm}}^2} \ll |U_{e4}|\sqrt{\Delta m_s^2} \ll m_{\text{lightest}}$, $m_\beta^{\text{SNO−NO}}$ is completely determined by the value of m_{lightest}.

FIG. 3.   Kinematic mass m_β from tritium β decay in different scenarios of SNO-NO (top left), SNO-IO (top right), SIO-NO (bottom left), and SIO-IO (bottom right) for $\Delta m_s^2 = 10^{-4}$ eV^2 (green), $\Delta m_s^2 = 0.01$ eV^2 (red), and $\Delta m_s^2 = 1.3$ eV^2 (blue).

TABLE IV. 3σ ranges of different combinations of oscillation parameters relevant to understanding kinematic mass (m_β) in the $3+1$ scenario.

$|U_{e2}|^2 \Delta m_{sol}^2$ $\times 10^{-5}$	$(1-|U_{e2}|^2)\Delta m_{sol}^2$ $\times 10^{-5}$	$|U_{e3}|^2 \Delta m_{atm}^2$ $\times 10^{-5}$	$|U_{e4}|^2 \Delta m_s^2$		
			$\Delta m_s^2 = 10^{-4}$ eV^2	$\Delta m_s^2 = 0.01$ eV^2	$\Delta m_s^2 = 1.3$ eV^2
(1.77:2.65)	(4.57:5.95)	(4.86:6.24)	$(1:2)\times 10^{-5}$	$(0.5:5)\times 10^{-5}$	$(0.13:1.3)\times 10^{-2}$

(4) SNO-IO:

$$m_\beta^{\text{SNO-IO}} \approx \sqrt{m_{\text{lightest}}^2 + \Delta m_{\text{atm}}^2 + |U_{e4}|^2 \Delta m_s^2}. \qquad (18)$$

(a) For $m_{\text{lightest}} \ll \Delta m_{\text{sol}}^2 < \Delta m_{\text{atm}}^2$, $m_\beta^{\text{SNO-IO}} \approx \sqrt{\Delta m_{\text{atm}}^2} \approx 0.05$ eV for $\Delta m_s^2 = 10^{-4}$ eV^2 and 0.01 eV^2 as $|U_{e4}|^2$ is very small. For $\Delta m_s^2 = 1.3$ eV^2, the value of $m_\beta^{\text{SNO-IO}} \approx \sqrt{\Delta m_{\text{atm}}^2 + |U_{e4}|^2 \Delta m_s^2}$. Thus, the value of m_β for $\Delta m_s^2 = 1.3$ eV^2 is greater than the $\sqrt{\Delta m_{\text{atm}}^2}$ till $m_2 \approx 0.1$ eV.

(b) $0.1 \ll m_{\text{lightest}}$, $m_\beta^{\text{SNO-IO}} \approx m_{\text{lightest}}$ for the values of Δm_s^2. Hence, for higher m_{lightest}, the behavior of m_β is fully characterized by m_{lightest}.

(5) SIO-NO:

$$m_\beta^{\text{SIO-NO}} = \sqrt{m_{\text{lightest}}^2 + \Delta m_s^2 + |U_{e2}|^2 \Delta m_{\text{sol}}^2 + |U_{e3}|^2 \Delta m_{\text{atm}}^2}. \qquad (19)$$

(a) For $m_{\text{lightest}} \ll \sqrt{\Delta m_{\text{sol}}^2} \ll \sqrt{\Delta m_{\text{atm}}^2}$, $m_\beta^{\text{SIO-NO}} \approx \sqrt{\Delta m_s^2}$ for $\Delta m_s^2 = 0.01$ eV^2 and 1.3 eV^2. For $\Delta m_s^2 = 10^{-4}$ eV^2, second and third term vary $\sim 10^{-5}$, so we get a small variation due to that.

(b) For $\sqrt{\Delta m_s^2} \ll m_{\text{lightest}}$, $m_\beta^{\text{SIO-NO}} \approx m_{\text{lightest}}$, and the value of $m_\beta^{\text{SIO-NO}}$ depend on m_{lightest} only.

(6) SIO-IO:

(a) For $\Delta m_s^2 > \Delta m_{\text{atm}}^2$, $m_\beta^{\text{SIO-IO}}$ can be written as

$$m_\beta^{\text{SIO-IO}} = \sqrt{m_{\text{lightest}}^2 + \Delta m_s^2} \qquad (20)$$

In this case, the conclusions are similar to SIO-NO for $\Delta m_s^2 = 0.01$ eV^2 and 1.3 eV^2.

(b) For $\Delta m_s^2 < \Delta m_{\text{atm}}^2$, $m_{\beta\beta}^{\text{SIO-IO}}$ can be expressed as

$$m_\beta^{\text{SIO-IO}} = \sqrt{m_{\text{lightest}}^2 + \Delta m_{\text{atm}}^2} \qquad (21)$$

In this case, for lower $m_{\text{lightest}} (< \sqrt{\Delta m_{\text{atm}}^2})$ region, $m_\beta^{\text{SIO-IO}} \approx \sqrt{\Delta m_{\text{atm}}^2} \approx 0.05$ eV. For higher values of $m_{\text{lightest}} (> \sqrt{\Delta m_{\text{atm}}^2})$, the value of $m_\beta^{\text{SNO-IO}}$ is proportional to m_{lightest} which leads to a straight line behavior in the figures.

The expressions of m_β^2 in various m_{lightest} limits are tabulated in Table IX in the Appendix.

C. Bound from neutrinoless double-beta decay

The cosmological observations and the tritium decay measurements are sensitive to the absolute neutrino mass scale, not to the nature of the neutrinos, i.e., whether the neutrinos are Dirac or Majorana. The neutrinoless double-beta decay ($0\nu\beta\beta$) process can provide both pieces of information. The $0\nu\beta\beta$ decay process constrains the half-life of the decaying isotope, which can be expressed as

$$T_{1/2} = \frac{m_e^2}{G_{0\nu} |\mathcal{M}_{0\nu}|^2 m_{\beta\beta}^2}, \qquad (22)$$

where m_e is electron mass, $G_{0\nu}$ denotes the leptonic phase space and $\mathcal{M}_{0\nu}$ is the nuclear transition matrix element of the decay and $m_{\beta\beta}$ is the effective Majorana mass which can be expressed as

$$\mathbf{m}_{\beta\beta} = \sum_i U_{ei}^2 m_i, \qquad (23)$$

where i runs over the light neutrino species.

The current upper limits are $m_{\beta\beta} \leq (36\text{–}156)$ meV and $(79\text{–}180)$ meV as reported by the KamLAND-Zen and GERDA experiments respectively. Recently, it was pointed out that the nuclear matrix element calculations should include a short-range contribution that originated from the hard-neutrino exchange mechanism described in [58,59]. Reference [60] showed that the inclusion of the short-range contribution tightens the limit on $m_{\beta\beta}$ as $m_{\beta\beta} \leq (25\text{–}68)$ meV for KamLAND-Zen.

1. Standard three-flavor framework

In the standard three-flavor framework Eq. (23) can be expressed as

$$\mathbf{m}_{\beta\beta}^{\text{Std}} = m_1 c_{12}^2 c_{13}^2 + m_2 s_{12}^2 c_{13}^2 e^{i\alpha} + m_3 s_{13}^2 e^{i\beta}. \qquad (24)$$

Unlike neutrino oscillation experiments, the effective Majorana mass is sensitive to the Majorana phases of the neutrinos. In addition, the effective Majorana mass is also sensitive to the mass orderings.

In Figs. 4–6, gray, and light brown regions display the effective mass governing $0\nu\beta\beta$ as a function of the lowest mass in the standard three-flavor framework for NO and IO, respectively. In these figures, the oscillation parameters are varied over their 3σ ranges as tabulated in Table I, and Majorana phases (α, β) are varied between $(0 : \pi)$.
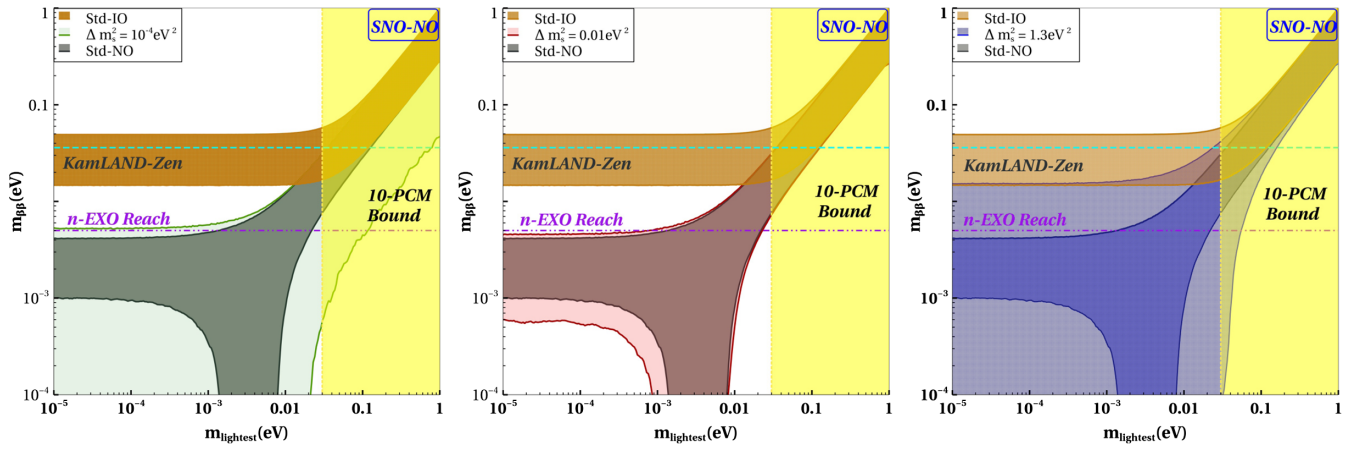
FIG. 4. $m_{\beta\beta}$ is plotted for SNO-NO (green) scenario against the lightest neutrino mass with the mass squared difference $(\Delta m_s^2) = 10^{-4}$ eV^2 (green), 0.01 eV^2 (red), and 1.3 eV^2 (blue) along with standard three-flavor NO (gray) and IO (brown).
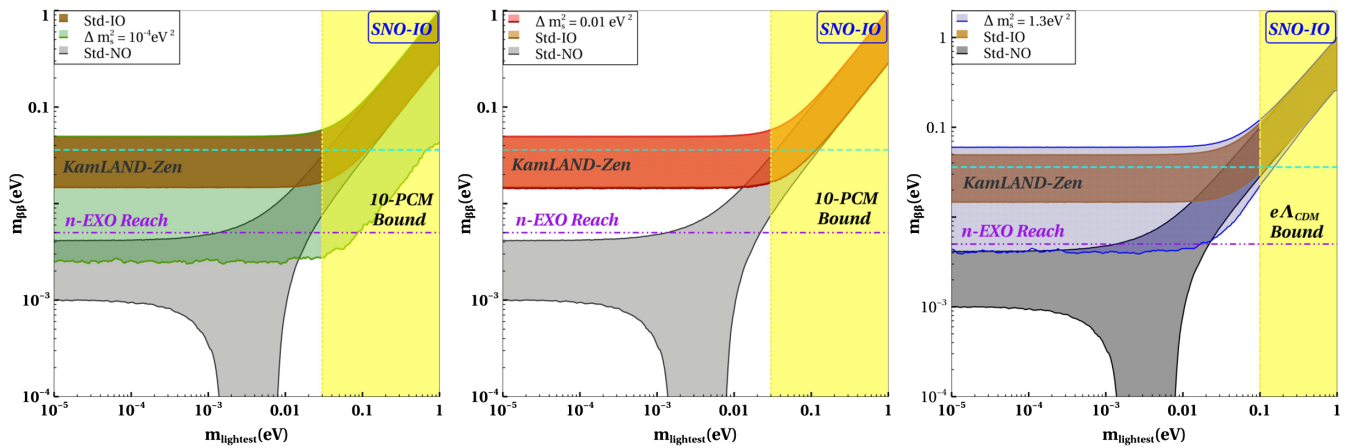
FIG. 5. $m_{\beta\beta}$ is plotted for SNO-IO scenario against the lightest neutrino mass with the mass squared difference $(\Delta m_s^2) = 10^{-4}$ eV^2 (green), 0.01 eV^2 (red), 1.3 eV^2 (blue) along with standard three-flavor normal ordering (gray) and inverted ordering (brown).
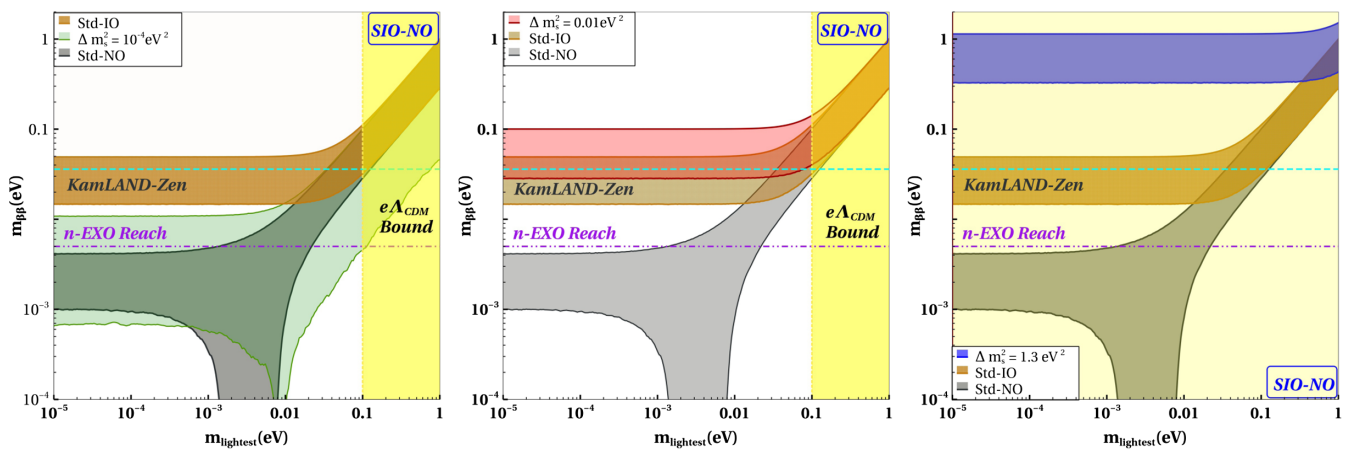
FIG. 6. $m_{\beta\beta}$ is plotted for SIO-NO (green) scenario against the lightest neutrino mass with the mass-squared difference $(\Delta m_s^2) = (10^{-4}$ eV$^2, 0.01$ eV$^2, 1.3$ eV$^2)$ along with standard three-flavor normal ordering (red) and inverted ordering (yellow).

TABLE V. 3σ ranges of different combinations of oscillation parameters relevant to understanding the effective Majorana mass in the standard three-flavor scenario.

Parameter	$\sqrt{r}$	$\sqrt{r}s_{12}^2$	$\sqrt{r}\cos 2\theta_{12}$	t_{13}^2	$\sqrt{r}t_{13}^2$
Max	0.18	0.0614	0.0828	0.0246	0.00443
Min	0.16	0.0432	0.0509	0.0204	0.00326

Normal ordering ($m_1 < m_2 < m_3$).—

(i) For $m_{\text{lightest}}(m_1) \ll \sqrt{\Delta m_{\text{sol}}^2} \ll \sqrt{\Delta m_{\text{atm}}^2}$, $m_2 \approx \sqrt{\Delta m_{\text{sol}}^2} \approx 0.01$ eV and $m_3 \approx \sqrt{\Delta m_{\text{atm}}^2} \approx 0.05$ eV. The effective Majorana mass can be approximated as

$$\mathbf{m}_{\beta\beta}^{\text{Std-NO}} = \sqrt{\Delta m_{\text{atm}}^2}c_{13}^2\left(\sqrt{r}s_{12}^2 e^{i\alpha} + t_{13}^2 e^{i\beta}\right), \quad (25)$$

where $r = \frac{\Delta m_{\text{sol}}^2}{\Delta m_{\text{atm}}^2}$. Complete cancellation is possible if $\sqrt{r}s_{12}^2 = t_{13}^2$. In Table V, we enlist different combinations of parameters appearing in the expression of $\mathbf{m}_{\beta\beta}^{\text{Std-NO}}$. As can be seen from the Table V, the maximum value of t_{13}^2 is much less than $\sqrt{r}s_{12}^2$, so complete cancellation is not possible in this region. For $\alpha = \beta = 0$, we get the highest value of $\mathbf{m}_{\beta\beta}^{\text{Std-NO}}$, while the lowest value is obtained for $\alpha = 0$, $\beta = \pi$, or $\alpha = \pi$, $\beta = 0$. In this region, the effective mass satisfies 0.001 eV $\lesssim |\mathbf{m}_{\beta\beta}^{\text{Std-NO}}| \lesssim 0.004$ eV.

(ii) For $m_{\text{lightest}} \approx \sqrt{\Delta m_{\text{sol}}^2}$. Here, $\mathbf{m}_{\beta\beta}^{\text{Std-NO}}$ can be expressed as

$$\mathbf{m}_{\beta\beta}^{\text{Std-NO}} = \sqrt{\Delta m_{\text{atm}}^2}c_{13}^2\left(\sqrt{r}c_{12}^2 + \sqrt{r}s_{12}^2 e^{i\alpha} + t_{13}^2 e^{i\beta}\right). \quad (26)$$

The effective mass attains minimum value for $\alpha = \beta = \pi$ and complete cancellation occurs when $\sqrt{r}\cos 2\theta_{12} = t_{13}^2$ From Table V, it can be inferred that complete cancellation is not possible in this region, which is also observed in Figs. 4–6.

(iii) From Fig. 4, it can seen that the value of $m_{\beta\beta}$ is very small in a region 0.002 eV $\lesssim \text{m}_{\text{lightest}} \lesssim 0.007$ eV. This region is commonly referred to as the cancellation region. As an example, considering the mixing parameters equal to their best fit values and $m_{\text{lightest}} = 0.005$ eV, we get $m_{\beta\beta} \approx 10^{-4}$ for the Majorana phases $\alpha = \beta = \pi$.

Inverted ordering ($m_3 < m_1 < m_2$).—

(i) In the limit $m_3 \approx 0$, $m_1 \approx m_2 \approx \sqrt{\Delta m_{\text{atm}}^2}$ and the effective mass can be expressed as

$$\mathbf{m}_{\beta\beta}^{\text{Std-IO}} = \sqrt{\Delta m_{\text{atm}}^2}c_{13}^2\left(c_{12}^2 + s_{12}^2 e^{i\alpha}\right). \quad (27)$$

In this region, $\mathbf{m}_{\beta\beta}^{\text{Std-IO}}$ is bounded from below and above by minimum and maximum values as

$$|\mathbf{m}_{\beta\beta}^{\text{Std-IO}}|_{\min} = \sqrt{\Delta m_{\text{atm}}^2}c_{13}^2 \cos 2\theta_{12} = 0.02 \text{ eV},$$

$$|\mathbf{m}_{\beta\beta}^{\text{Std-IO}}|_{\max} = \sqrt{\Delta m_{\text{atm}}^2}c_{13}^2 = 0.05 \text{ eV}. \quad (28)$$

These bounds are reflected also in Figs. 4–6.

Quasidegenerate spectrum ($m_1 \approx m_2 \approx m_3 \gtrsim 0.05$ eV).— The region where $m_{\text{lightest}} \gtrsim \sqrt{\Delta m_{\text{atm}}^2} \gtrsim 0.05$ eV (for both mass orderings), m_1, m_2, and m_3 are approximately equal. This region is called the quasidegenerate region. Here the effective mass can be expressed as

$$\mathbf{m}_{\beta\beta}^{\text{QD}} = m_0 c_{13}^2(c_{12}^2 + s_{12}^2 e^{i\alpha} + t_{13}^2 e^{i\beta}). \quad (29)$$

In this region, cancellation is not possible, as $t_{13}^2 \approx 0.02$, $s_{12}^2 \approx 0.3$ will not be able to cancel out $c_{12}^2 \approx 0.7$ as can be seen from Figs. 4–6. This region is in serious tension with the cosmological observations because, for three degenerate neutrinos, the bound on $m_{\text{lightest}} < 0.05$ eV considering $\sum m_\nu < 0.16$ eV [from Eq. (13)].

2. 3 + 1 framework

In this subsection, the behavior of $m_{\beta\beta}$ is studied in the context of various mass ordering schemes in the presence of a light sterile neutrino. The plots in Figs. 4–7 are generated by allowing all the oscillation parameters to vary in their 3σ range as mentioned in Table I, and the sterile parameters are varied according to the Table II.

SNO-NO.— The effective Majorana mass in this scenario can be written as

$$m_{\beta\beta}^{\text{SNO-NO}} = c_{14}^2\left|\mathbf{m}_{\beta\beta}^{\text{Std-NO}} + t_{14}^2 m_4 e^{i\gamma}\right|, \quad (30)$$

where $\mathbf{m}_{\beta\beta}^{\text{Std-NO}}$ is the standard three-flavor effective mass for normal ordering. In Fig. 4, we plotted $m_{\beta\beta}^{\text{SNO-NO}}$ as a function of the lightest neutrino mass ($m_{\text{lightest}} = m_1$) for the three mass-squared differences. To explain the behavior of $m_{\beta\beta}^{\text{SNO-NO}}$ in Fig. 4, we consider different limits of m_{lightest}.

The values of different terms in Eq. (30) are mentioned for various limits of m_1 in the Table VI where the maximum value of $m_{\beta\beta}^{\text{SNO-NO}}$ corresponds to $\gamma = 0$ and minimum is for $\gamma = \pi$. The important points are as follows:

(i) For $m_1 \ll \sqrt{\Delta m_{\text{sol}}^2} \ll \sqrt{\Delta m_{\text{atm}}^2} \ll \sqrt{\Delta m_s^2}$, it is seen from Table VI that for $\Delta m_s^2 = 10^{-4}, 1.3$ eV^2 complete cancellation is possible between $\mathbf{m}_{\beta\beta}^{\text{Std-NO}}$ and $m_4 t_{14}^2$ for $\gamma = \pi$.

TABLE VI. 3σ ranges of different combinations of oscillation parameters relevant to understanding the effective Majorana mass for SNO-NO in the $3+1$ framework.

Regions	$\mathbf{m}_{\beta\beta}^{\text{Std-NO}}$ (eV)	$\|m_4 t_{14}^2\|$ (eV)		
		$\Delta m_s^2 = 10^{-4}$ eV^2	$\Delta m_s^2 = 0.01$ eV^2	$\Delta m_s^2 = 1.3$ eV^2
$m_1 \approx 0$	0.001:0.004	0.001:0.002	$5 \times 10^{-5}:10^{-4}$	0.001:0.01
$m_1 \approx \sqrt{\Delta m_{\text{sol}}^2}$	0.0018:0.018	0.0014:0.003	$5 \times 10^{-5}:10^{-4}$	0.001:0.01
$m_1 \approx 0.1$	0.02:0.1	0.01:0.02	$5 \times 10^{-4}:10^{-3}$	0.001:0.01

  (ii) For $m_1 \approx \sqrt{\Delta m_{\text{sol}}^2}$, complete cancellations continue to occur for $\Delta m_s^2 = 10^{-4}$ eV^2 and 1.3 eV^2.
 (iii) At higher values of $m_1 \approx 0.1$ eV, complete cancellation happens only for $\Delta m_s^2 = 10^{-4}$ eV^2 as seen from third row.
 (iv) In the $3+1$ scenario quasidegenerate (QD) condition will arise when $m_1 \approx m_2 \approx m_3 \approx m_4$. As seen in Fig. 12(a), the QD region occurs around 0.08 eV, 0.2 eV for $\Delta m_s^2 = 10^{-4}, 0.01$ eV^2. KamLAND-Zen and nEXO both can probe a fraction of the QD region for $\Delta m_s^2 = 10^{-4}$ eV^2 and the entire region for $\Delta m_s^2 = 0.01$ eV^2. However, cosmological bounds ($m_1 > 0.03$ eV) reject the QD region for both values of Δm_s^2.

SNO-IO.—Effective Majorana mass from double beta decay can be expressed as

$$m_{\beta\beta}^{\text{SNO-IO}} = c_{14}^2 \left| \mathbf{m}_{\beta\beta}^{\text{Std-IO}} + t_{14}^2 m_4 e^{i\gamma} \right|. \qquad (31)$$

We have plotted $m_{\beta\beta}^{\text{SNO-IO}}$ as a function of the lightest neutrino mass (m_3) for the three mass-squared differences in the Fig. 5. The values of the terms in Eq. (31) are listed in Table VII.

The notable points in the SNO-IO case are as follows:
  (i) It is evident from Table VII, that the minimum value of $\mathbf{m}_{\beta\beta}^{\text{Std-IO}}$ is always greater than the maximum value of $m_4 t_{14}^2$ for all the three mass-squared differences. Hence, complete cancellation is not possible for the entire range of m_{lightest}.
 (ii) The value of $m_4 t_{14}^2$ for $\Delta m_s^2 = 0.01$ eV^2 is very small compared to $\mathbf{m}_{\beta\beta}^{\text{Std-IO}}$. Therefore, $m_{\beta\beta}^{\text{SNO-IO}}$ is approximately equal to $\mathbf{m}_{\beta\beta}^{\text{Std-IO}}$ which is visible from the middle panel of Fig. 5.
 (iii) For $\Delta m_s^2 = 10^{-4}$ eV^2 and 1.3 eV^2, the minimum value of $m_{\beta\beta}^{\text{SNO-IO}} \approx 0.01$ eV is attained for $\gamma = \pi$ which can be probed partially in the future experiment, nEXO.
 (iv) The QD regions, as observed from Fig. 13, is occurred at $m_3 > 0.1$, 0.2 eV for $\Delta m_s^2 = 10^{-4}$, 0.01 eV^2 respectively. Although the QD region is disfavored by cosmology for both the Δm_s^2 values, KamLAND-Zen and nEXO can probe this region partially for $\Delta m_s^2 = 10^{-4}$ eV^2 and completely for $\Delta m_s^2 = 0.01$ eV^2.

SIO-NO.—The effective Majorana mass is expressed as

$$m_{\beta\beta}^{\text{SIO-NO}} \approx c_{14}^2 \left(\sqrt{m_4^2 + \Delta m_s^2}(c_{12}^2 + s_{12}^2 e^{i\alpha}) + m_4 t_{14}^2 e^{i\gamma} \right), \qquad [\Delta m_s^2 > \Delta m_{\text{atm}}^2]$$

$$m_{\beta\beta}^{\text{SIO-NO}} \approx c_{14}^2 \left(c_{13}^2 \left(\sqrt{m_4^2 + \Delta m_s^2}(c_{12}^2 + s_{12}^2 e^{i\alpha}) + \sqrt{m_4^2 + \Delta m_{\text{atm}}^2} s_{13}^2 e^{i\beta} \right) + m_4 t_{14}^2 e^{i\gamma} \right) \qquad [\Delta m_s^2 < \Delta m_{\text{atm}}^2]. \qquad (32)$$

Here, we have used the mass relations mentioned in Eq. (10). In Fig. 6, we have shown $m_{\beta\beta}$ as function of m_{lightest} (m_4) in three panels corresponding to different values of Δm_s^2. Table VIII depicts the terms of Eq. (32).

TABLE VII. The 3σ ranges of different combinations of oscillation parameters relevant to understanding the effective Majorana mass for SNO-IO in the $3+1$ framework.

Regions	$\mathbf{m}_{\beta\beta}^{\text{Std-IO}}$ (eV)	$m_4 t_{14}^2$ (eV)		
		$\Delta m_s^2 = 10^{-4}$ eV^2	$\Delta m_s^2 = 0.01$ eV^2	$\Delta m_s^2 = 1.3$ eV^2
$m_3 \approx 0$	0.02:0.05	0.005:0.01	$5 \times 10^{-5}:5 \times 10^{-4}$	0.001:0.01
$m_3 \approx 0.1$	0.03:0.1	0.01:0.025	$7.5 \times 10^{-5}:7.5 \times 10^{-4}$	0.001:0.01

TABLE VIII. The 3σ ranges of different combinations of oscillation parameters relevant to understanding the effective Majorana mass for SIO-NO in the $3+1$ framework.

| Regions | $\sqrt{\Delta m_s^2}\cos 2\theta_{12}$ (eV) | | | $\sqrt{\Delta m_{\text{atm}}^2}t_{13}^2$ (eV) | $m_4 t_{14}^2$ (eV) | | |
	$\Delta = 10^{-4}$	$\Delta = 0.01$	$\Delta = 1.3$		$\Delta = 10^{-4}$	$\Delta = 0.01$	$\Delta = 1.3$
$m_4 \approx 0$	0.003	0.03	0.33	0.001	0	0	0
$m_4 \approx 0.01$	0.003	0.03	0.33	0.001	$0.001:0.002$	$5.10^{-5}:5.10^{-4}$	$10^{-5}:10^{-4}$

(i) For the region where the lightest mass is negligible (see Fig. 14), Eq. (10) will be

$$m_4 \approx 0, \qquad m_2 \approx m_1 \approx m_3 \approx \sqrt{\Delta m_s^2}, \qquad (\Delta m_s^2 > \Delta m_{\text{atm}}^2),$$

$$m_4 \approx 0, \qquad m_1 \approx m_2 \approx \sqrt{\Delta m_s^2}, \qquad m_3 \approx \sqrt{\Delta m_{\text{atm}}^2}, \qquad (\Delta m_s^2 < \Delta m_{\text{atm}}^2). \tag{33}$$

Effective Majorana mass from double beta decay

$$m_{\beta\beta}^{\text{SIO-NO}} = \sqrt{\Delta m_s^2}\left(c_{12}^2 + s_{12}^2 e^{i\alpha}\right), \qquad (\Delta m_s^2 > \Delta m_{\text{atm}}^2),$$

$$m_{\beta\beta}^{\text{SIO-NO}} = c_{13}^2 c_{14}^2 \left(\sqrt{\Delta m_s^2}\left(c_{12}^2 + s_{12}^2 e^{i\alpha}\right) + \sqrt{\Delta m_{\text{atm}}^2}t_{13}^2 e^{i\beta}\right), \qquad (\Delta m_s^2 < \Delta m_{\text{atm}}^2). \tag{34}$$

In the first case, complete cancellation can happen for $\alpha = \pi$ and $c_{12}^2 = s_{12}^2$, but since θ_{12} is less than 45°, this cannot happen, as shown in Fig. 6 for $\Delta m_s = 10^{-4}$ eV^2. In the second case, complete cancellation occurs for $\alpha = \beta = \pi$ and

$$\sqrt{\Delta m_s^2}\cos 2\theta_{12} = \sqrt{\Delta m_{\text{atm}}^2}t_{13}^2. \tag{35}$$

This condition is not satisfied for $\Delta m_s^2 = 1.3$, 0.01 eV^2 as can be seen from Table I and Table VIII. The value of $m_{\beta\beta}^{\text{SIO-NO}}$ varies between $(0.3:1)$ eV and $(0.001:0.01)$ eV for $\Delta m_s^2 = 1.3, 10^{-4}$ eV^2, respectively, as seen in Fig. 6.

(ii) Around $m_4 \approx 0.01$ eV, in case of $\Delta m_s^2 = 0.01$ eV^2 and 1.3 eV^2, the sterile contribution is negligible compared to other terms as the value of θ_{14} is small and thus no cancellation occurs, but due to large θ_{14} for $\Delta m_s^2 = 10^{-4}$, the value of $m_4 t_{14}^2$ varies between $(0.001:0.002)$ which allows us to have a narrow cancellation region for $\alpha = \beta = \gamma = \pi$.

(iii) It is to be noted that the KamLAND-ZEN experiment disallows the entire parameter space of $m_{\beta\beta}^{\text{SIO-NO}}$ for $\Delta m_s^2 = 1.3$ eV^2. For $\Delta m_s^2 = 0.01$ eV^2 a part of the parameter space gets disfavored for all values of m_{lightest}, whereas for $\Delta m_s^2 = 10^{-4}$ eV^2 regions with higher values of $m_{\text{lightest}}(> 0.3$ eV$)$ are disfavored. For 10^{-4} eV^2, the allowed region of $m_{\beta\beta}^{\text{SIO-NO}}$ can be partially probed by nEXO experiment.

SIO-IO.—In three panels of Fig. 7, the Majorana mass, $m_{\beta\beta}$ in SIO-IO scenario has been plotted against $m_{\text{lightest}} = m_4$.

(i) For $\Delta m_s^2 > \Delta m_{\text{atm}}^2$, $m_{\beta\beta}$ is exactly similar to the SIO-NO scenario ($\Delta m_s^2 > \Delta m_{\text{atm}}^2$). Thus, the results and the conclusions remain identical.

(ii) For $\Delta m_s^2 < \Delta m_{\text{atm}}^2$, the value of $m_{\beta\beta}$ in a region where m_{lightest} is small, can be approximated as

$$\left(m_{\beta\beta}^{\text{SIO-IO}}\right)_{\Delta m_s^2 < \Delta m_{\text{atm}}^2}$$
$$= \sqrt{\Delta m_{\text{atm}}^2}c_{14}^2\left(c_{12}^2 + s_{12}^2 e^{i\alpha} + t_{14}^2 e^{i\gamma}\right). \tag{36}$$

Here, complete cancellation requires $\alpha = \gamma = \pi$ and

$$\cos 2\theta_{12} = t_{14}^2. \tag{37}$$

In this region, complete cancellation is not possible as Eq. (37) is not satisfied for the allowed range of mixing angle θ_{14} given in Table II.

(iii) As can be seen in Fig. 15, for $m_{\text{lightest}} > \sqrt{\Delta m_{\text{atm}}^2}$, $m_1 \approx m_2 \approx m_3 \approx m_4 \approx m_0$ and the value of $m_{\beta\beta}$ can be written as

$$\left(m_{\beta\beta}^{\text{SIO-IO}}\right)_{\Delta m_s^2 < \Delta m_{\text{atm}}^2} = m_0 c_{14}^2\left(c_{12}^2 + s_{12}^2 e^{i\alpha} + t_{14}^2 e^{i\gamma}\right) \tag{38}$$

In this region, cancellation is also not possible, and $m_{\beta\beta}$ is proportional to the value of the lightest mass.

(iv) It can be seen from Fig. 7, higher values of $m_{\beta\beta}$ are disfavored by KamLAND-Zen for all values of m_{lightest} and nEXO can rule out an even greater part of the parameter space in the absence of any signal.
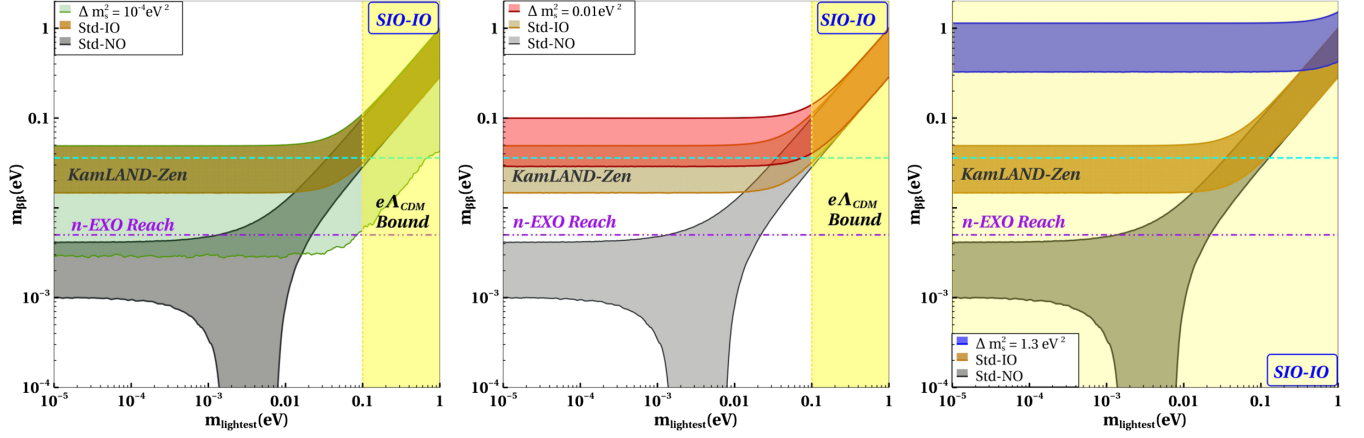
FIG. 7. $m_{\beta\beta}$ is plotted for SIO-IO (green) scenario against the lightest neutrino mass with the mass squared difference $(\Delta m_s^2) = (10^{-4} \text{ eV}^2, 0.01 \text{ eV}^2, 1.3 \text{ eV}^2)$ along with standard three-flavor normal ordering (red) and inverted ordering (yellow).

The expressions of $m_{\beta\beta}$ in various $m_{lightest}$ limits are tabulated in Table X in the Appendix.

D. Correlations

In the earlier subsections, we discussed the independent constraints on mass variables from cosmology, single β decay, and $0\nu\beta\beta$ decay. In this section, we discuss the correlations of the mass observable amongst each other [61]. We have plotted in Figs. 8–11, the correlation of m_β against Σ (left), $m_{\beta\beta}$ against Σ (middle), and $m_{\beta\beta}$ against m_β (right) for all the mass spectra. The yellow-shaded and the brown-hatched regions correspond to cosmologically excluded regions mentioned in Eqs. (13) and (14), respectively. The other horizontal and vertical lines are the current experimental limits [KamLAND-Zen (Cyan)] and future sensitivity [KATRIN (Pink), Project 8 (Black), nEXO (Magenta)] with their respective color mentioned in brackets. Blue, red, and green regions in the plots

of Figs. 8–11 correspond to $\Delta m_s^2 = 1.3 \text{ eV}^2$, 0.01 eV^2, 10^{-4} eV^2, respectively. For each value of Δm_s^2, the mixing angles and mass squared differences are varied within the 3σ range mentioned in Table I and Table II. The lightest neutrino mass and the Majorana phases are varied over $(10^{-5} : 1)$ eV and $(0 : \pi)$, respectively. The nature of the plots can be understood from the plots of Σ, m_β, $m_{\beta\beta}$ presented earlier. For instance, the left most panel is the correlation plot in the $m_\beta - \Sigma$ plane. From Figs. 2 and 3 it is seen that for SNO-NO and $\Delta m_s^2 = 1.3 \text{ eV}^2$, Σ is in the range $\sim(0.3 : 3)$ eV while m_β is in the range $\sim(0.04 : 1)$ eV. This is reflected in the blue shaded regions in Fig. 8. For the $m_{\beta\beta}$ plots (middle and the right panels) the widths are due to the Majorana phases and correspond to the ranges obtained in Fig. 4. Similarly, for other mass spectra, the nature of the plots can also be explained by looking at the figures. Below, we describe the correlations among the different observables.
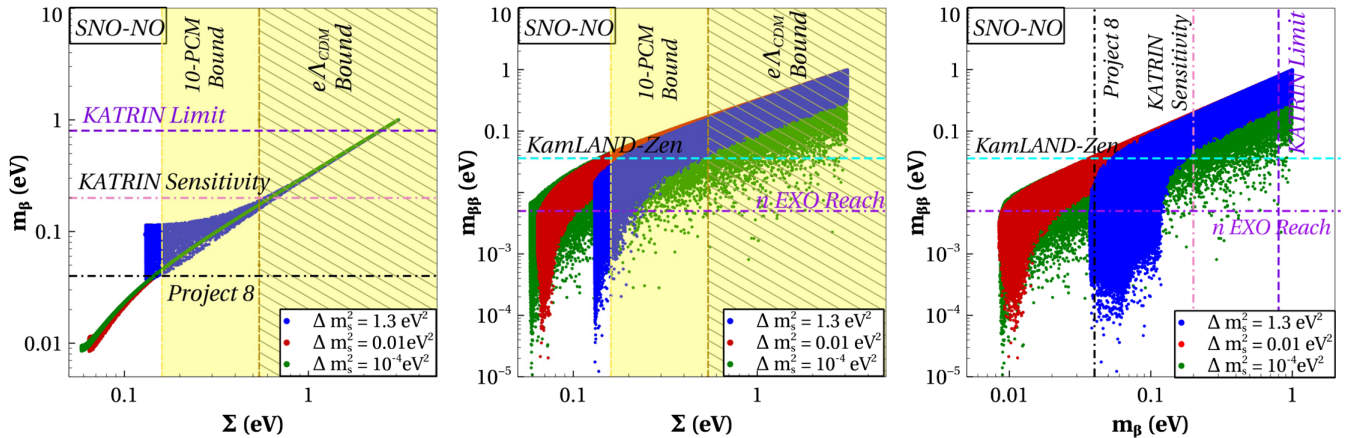
FIG. 8. Correlations of m_β against and Σ (left), $m_{\beta\beta}$ against Σ (middle), and $m_{\beta\beta}$ against m_β (right) for SNO-NO is plotted here. The green, blue, and red regions describe the values for $\Delta m_s^2 = 10^{-4} \text{ eV}^2$, 0.01 eV^2, and 1.3 eV^2, respectively. The yellow-shaded and brown-hatched regions correspond to the exclusion regions by Eqs. (13) and (14), respectively.
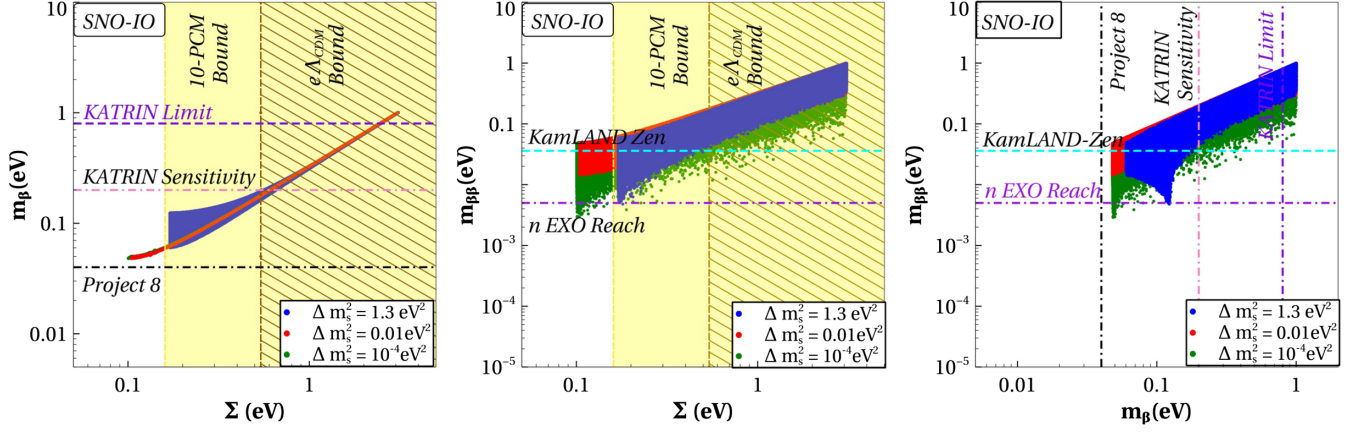
FIG. 9. Correlations of m_β against and Σ (left), $m_{\beta\beta}$ against Σ (middle), and $m_{\beta\beta}$ against m_β (right) for SNO-IO is plotted here. The green, blue, and red regions describe the values for $\Delta m_s^2 = 10^{-4}$ eV^2, 0.01 eV^2 and 1.3 eV^2, respectively. The yellow-shaded and brown-hatched regions correspond to the exclusion regions by Eqs. (13) and (14), respectively.
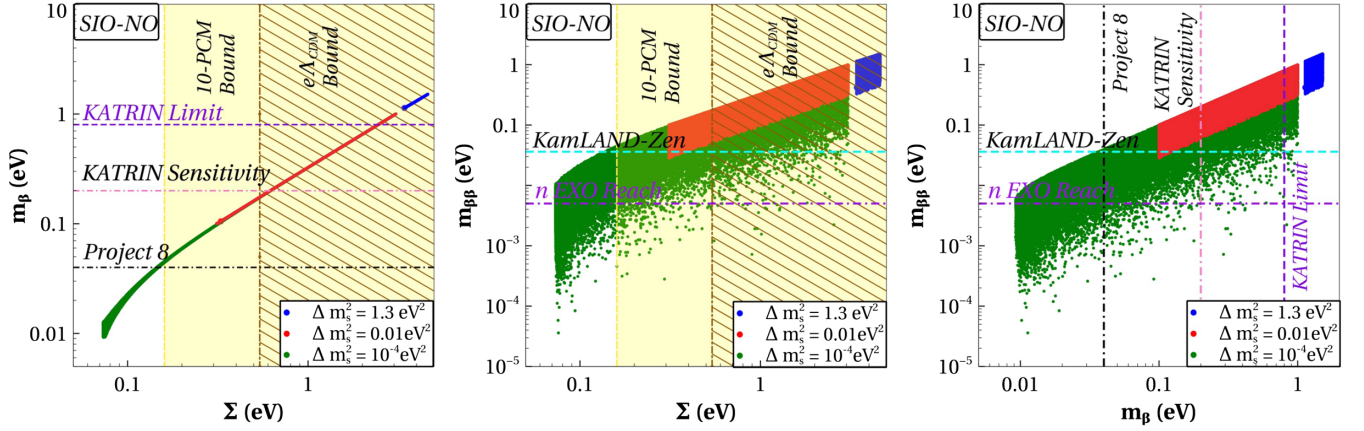
FIG. 10. Correlations of m_β against and Σ (left), $m_{\beta\beta}$ against Σ (middle), and $m_{\beta\beta}$ against m_β (right) for SNO-IO is plotted here. The green, blue, and red regions describe the values for $\Delta m_s^2 = 10^{-4}$ eV^2, 0.01 eV^2, and 1.3 eV^2, respectively. The yellow-shaded and brown-hatched regions correspond to the exclusion regions by Eqs. (13) and (14), respectively.
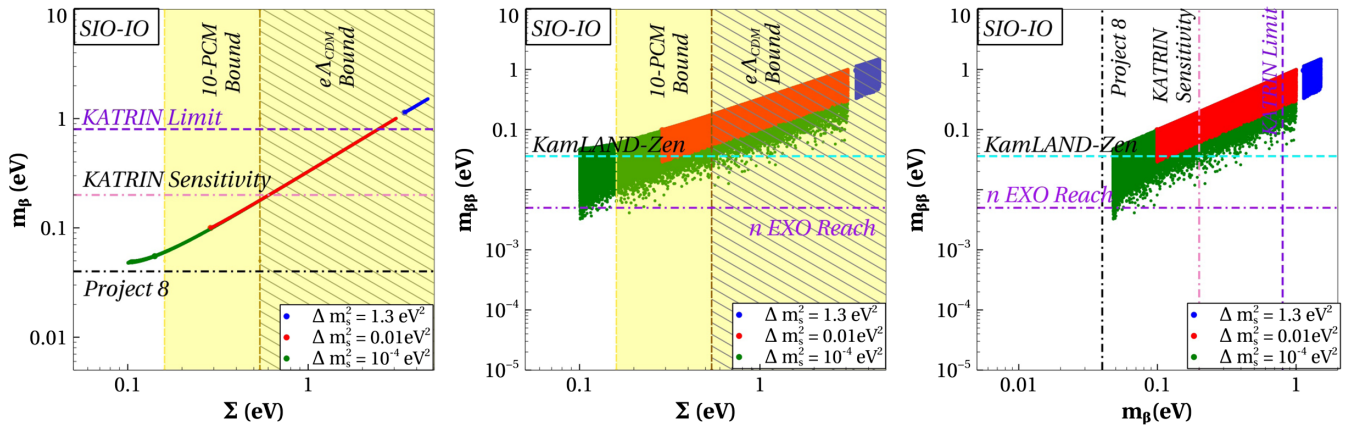
FIG. 11. Correlations of m_β against and Σ (left), $m_{\beta\beta}$ against Σ (middle), and $m_{\beta\beta}$ against m_β (right) is plotted here. The green, blue, black, and red regions describe SNO-NO, SNO-IO, SIO-NO, and SIO-IO, respectively. The shaded regions correspond to the exclusion regions of the respective x-axis labels.

(1) SNO-NO:

   The correlation plots for SNO-NO are shown in Fig. 8:

   (a) From the left panel, it is seen that the cosmological mass bound disfavors a large parameter space for all three mass-squared differences. The allowed region from cosmology will not be sensitive to KATRIN's projected limit, but the proposed Project 8 experiment can probe the parameter space for $\Delta m_s^2 = 1.3$ eV^2.

   (b) From the middle panel, it is observed that some part of the parameter space disfavored by the cosmological bound is also disfavored by KamLAND-Zen. In the region allowed by cosmology, m_β can be very low. Therefore, KamLAND-Zen can probe a very small part of it, and the projected sensitivity nEXO experiment can only probe some parts of these regions for all the mass-squared differences.

   (c) From the right panel, it can be noted that the proposed experiments nEXO and Project 8 together can rule out almost the entire parameter space for $\Delta m_s^2 = 1.3$ eV^2 in the absence of any signal. However, in the case of $\Delta m_s^2 = 0.01, 10^{-4}$ eV^2, only parts of the parameter space can be probed by the upcoming above cited experiments.

(2) SNO-IO:

   Figure 9 shows the correlation plots for SNO-IO:

   (a) From the left panel, it is visible that $\Delta m_s^2 = 1.3$ eV^2 is ruled out by stringent cosmological limit. But for $\Delta m_s^2 = 10^{-4}$ eV^2 and 0.01 eV^2 small parts of parameter space are allowed by cosmology and KATRIN's projected sensitivity. These allowed regions can be completely probed in the proposed Project 8 experiment.

   (b) It can be noted from the middle panel that KamLAND-Zen and cosmology rule out a large part of the parameter space for all the mass-squared differences. For $\Delta m_s^2 = 0.01, 10^{-4}$ eV^2, the region allowed by cosmology and KamLAND-Zen can be probed in future experiment nEXO.

   (c) From the right panel, it is observed that Project 8 and nEXO experiments together can probe the entire parameter space for $\Delta m_s^2 = 10^{-4}$ eV^2, 0.01 eV^2, and 1.3 eV^2.

(3) SIO-NO:

   In Fig. 10, correlations between the mass variables for the SIO-NO scenario are plotted:

   (a) The left and middle panels show that $e\Lambda_{\rm CDM}$ model only allows a part of the parameter space for $\Delta m_s^2 = 0.01$ eV^2, 10^{-4} eV^2, however with the cosmological bound only $\Delta m_s^2 = 10^{-4}$ eV^2 is preferred.

(b) From the left panel, it is visible that the current KATRIN bound cannot probe the regions allowed by cosmological and $e\Lambda_{\rm CDM}$ model. Only proposed Project 8 can probe allowed regions for 1.3 eV^2.

(c) The middle panel depicts that the KamLAND-Zen sensitivity will be able to probe the $e\Lambda_{\rm CDM}$ favored regions of 10^{-4} eV^2 and 0.01 eV^2 partially. The nEXO can completely probe allowed regions of 0.01 eV^2.

(d) It is to be noted from the right panel that the future experiments nEXO and Project 8 can together probe the entirety of the parameter space for $\Delta m_s^2 = 1.3$ eV^2, 0.01 eV^2, and a fraction of the regions for $\Delta m_s^2 = 10^{-4}$ eV^2.

(4) SIO-IO:

   The correlations amongst the mass variables for the SIO-IO scenario are plotted in Fig. 11:

   (a) From the left panel, we understand that the SIO-IO scenario is similar to the SIO-NO scenario. The only difference is that Project 8 will be able to probe the entire cosmologically allowed regions of $\Delta m_s^2 = 10^{-4}$ eV^2.

   (b) The middle panel portrays similar observations to that of SIO-NO apart from the fact that now future experiment nEXO can cover almost the total parameter space for all Δm_s^2 values considered by us.

   (c) From the right panel, it can be seen that the proposed experiments Project 8 and nEXO can together cover the entire parameter space for all the values of Δm_s^2.

IV. SUMMARY AND DISCUSSION

The results from short baseline neutrino oscillation experiments e.g., LSND and MiniBooNE and radiochemical experiments e.g., GALLEX, SAGE, and BEST indicate the possibility of having an extra neutrino state with $\mathcal{O}(\text{eV})$ mass squared difference. Moreover, the tension between the results of T2K and NOνA experiments can be improved by invoking an additional state mass squared difference $\sim 10^{-2}$ eV^2 and lack of upturn events in the solar neutrino spectra below 8 MeV can be explained by an ultralight sterile neutrino. Thus, sterile neutrinos with a very wide range of mass differences ($\Delta m_s^2 = m_4^2 - m_1^2$) have been proposed in the literature. The addition of a sterile state implies four mass spectra, namely: SNO-NO ($\Delta m_s^2 > 0, \Delta m_{\rm atm}^2 > 0$), SNO-IO ($\Delta m_s^2 > 0, \Delta m_{\rm atm}^2 < 0$), SIO-NO ($\Delta m_s^2 < 0, \Delta m_{\rm atm}^2 > 0$), and SIO-IO ($\Delta m_s^2 < 0, \Delta m_{\rm atm}^2 < 0$), where NO (IO) stands for +ve (−ve) value of Δm_{31}^2 and SNO (SIO) stand for +ve (−ve) value of Δm_{41}^2. The mass spectra are depicted in Fig. 1. We explore the implications of the mass spectra for sum of light neutrino masses from cosmology, beta decay, and $0\nu\beta\beta$ decay.

(i) The scenario of $\Delta m_s^2 = 1.3$ eV^2 with $\Delta m_s^2 < 0$ is known to be in conflict with the cosmological bound on the sum of neutrino masses. The specific bounds depend on the chosen datasets and the cosmological models used for fitting. Here we consider two different cosmological models; a 10 parameter cosmological model (10-PCM) and a 12 parameter cosmological model ($e\Lambda_{\mathrm{CDM}}$) which provide the limit on the total mass of the light neutrino species as $\sum < 0.16$ eV and $\sum < 0.52$ eV, respectively. We find that SIO-NO and SIO-IO is completely ruled out by cosmology. Moreover, such scenarios are disfavored from the current limit on m_β by KATRIN experiment and also from the upper limit on $m_{\beta\beta}$ by KamLAND-Zen experiment. We want to emphasize that SIO-NO and SIO-IO scenarios for $\Delta m_s^2 = 1.3$ eV^2 are not only disfavored by cosmology but also by KATRIN and KamLAND-Zen. However, we see that SNO-NO and SNO-IO for $\Delta m_s^2 = 1.3$ eV^2 is still allowed below $m_{\mathrm{lightest}} \approx 0.1$ eV, in the limit of $e\Lambda_{\mathrm{CDM}}$ model, KATRIN and KamLAND-Zen but proposed experiment Project 8 will be able to probe the scenarios with the projected limit of m_β.

(ii) It is often believed that sterile neutrinos with mass-squared difference smaller than 1.3 eV^2 can be allowed by cosmology. Here we find that, for $\Delta m_s^2 = 0.01$ eV^2, all mass spectra are allowed in $e\Lambda_{\mathrm{CDM}}$ model up to a value of $m_{\mathrm{lightest}} \approx 0.1$ eV but SIO-NO and SIO-IO is disfavored when 10-PCM model is considered whereas SNO-NO and SNO-IO scenarios remain valid up to $m_{\mathrm{lightest}} \sim 0.03$ eV. It is also noted that projected sensitivity from KATRIN experiments will not be able to probe the mass spectra, but SNO-IO, SIO-NO, and SIO-IO scenarios can be probed completely with Project 8's proposed sensitivity. In the case of neutrinoless double decay measurements, KamLAND-Zen experiment ruled out most of the parameter space of

SNO-NO and SIO-IO scenario for $\Delta m_s^2 = 0.01$ eV^2 and next generation experiment nEXO will be able to probe the parameter space completely. Moreover, nEXO will also be able to probe the SNO-IO scenario completely for $\Delta m_s^2 = 0.01$ eV^2.

(iii) It is seen from Fig. 2 that $\Delta m_s^2 = 10^{-4}$ eV^2 i.e., sterile neutrino with very small mass-squared difference is allowed up to $m_{\mathrm{lightest}} \approx 0.03$ eV and up to $m_{\mathrm{lightest}} \approx 0.1$ eV from $e\Lambda_{\mathrm{CDM}}$ model. In case of direct mass measurement, KATRIN's projected limit can probe the mass spectra up to $m_{\mathrm{lightest}} \approx 0.2$ eV whereas Project 8 will be able to probe SNO-IO, SIO-IO scenarios completely and SNO-NO, SIO-NO scenarios up to $m_{\mathrm{lightest}} \approx 0.04$ eV. We also find that neither KamLAND-Zen nor nEXO can completely probe the mass spectra, but they rule out some parameter space for SNO-IO, SIO-NO, and SIO-IO scenarios.

In conclusion, in the presence of a light sterile state, mass-related observables can provide constraints on the possible spectra and can disfavor some of these depending on the mass of the sterile state.

APPENDIX: MASS-SPECTRUM
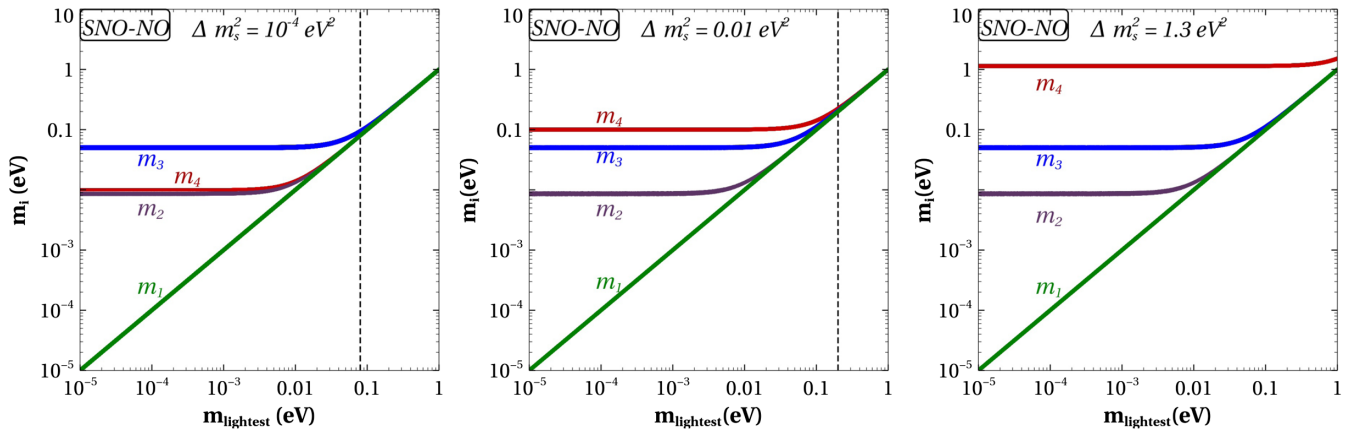
FIG. 12. Variation of masses with respect to the lightest neutrino mass for SNO-NO.
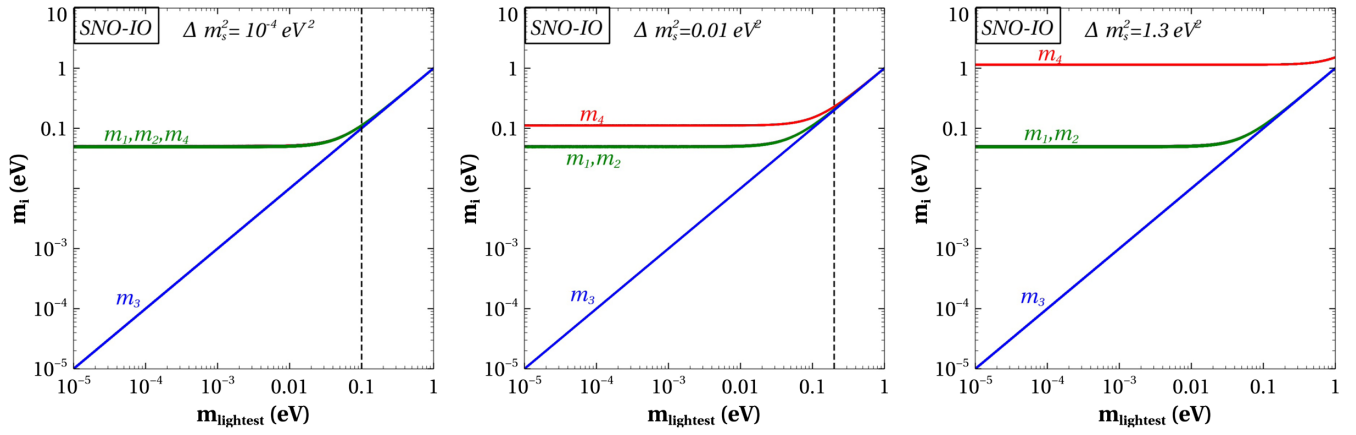
FIG. 13.   Variation of masses with respect to the lightest neutrino mass for SNO-IO.
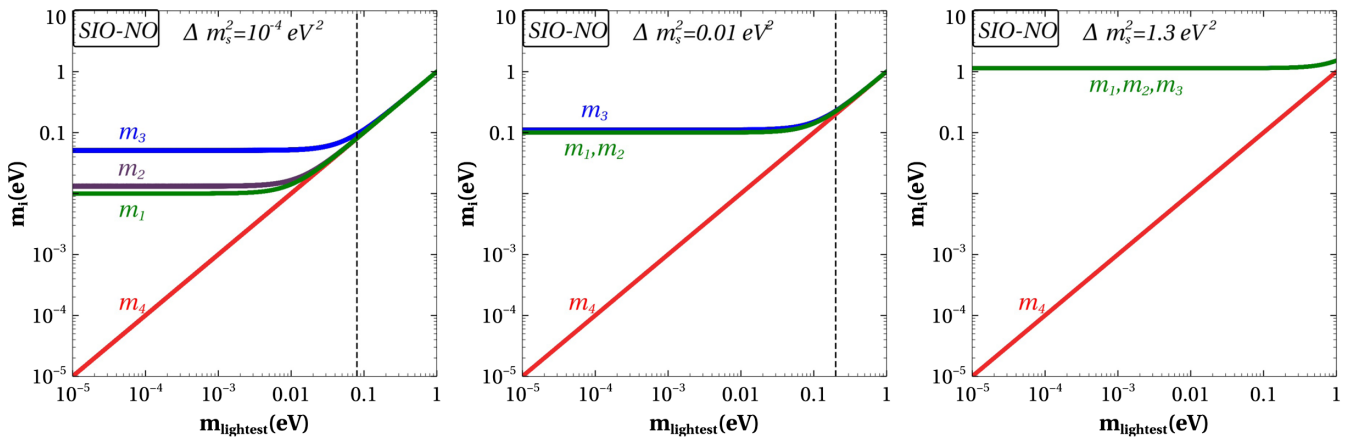
FIG. 14.   Variation of masses with respect to the lightest neutrino mass for SIO-NO.
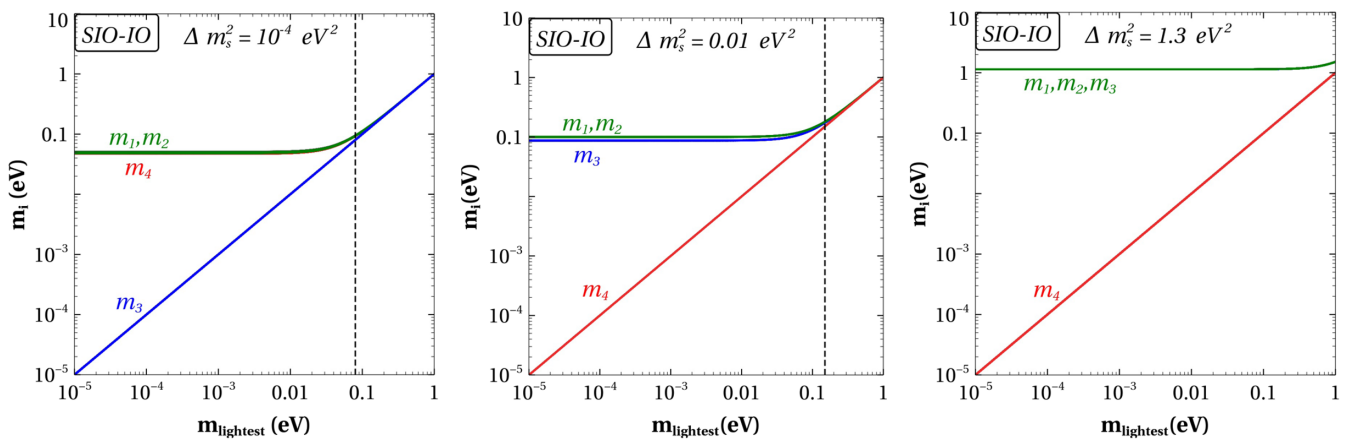
FIG. 15.   Variation of masses with respect to the lightest neutrino mass for SIO-IO.

TABLE IX. The table depicts expressions of m_β^2 in third, fourth, and fifth columns corresponding to $\Delta m_s^2 = 10^{-4}$, 10^{-2}, and 1.3 eV^2, respectively, for various mass spectra given in the first column under different regions shown in column two.

Mass Spectra	Region	Expression of m_β^2		
		(I) $\Delta m_s^2 = 10^{-4}$ eV^2	(II) $\Delta m_s^2 = 10^{-2}$ eV^2	(III) $\Delta m_s^2 = 1.3$ eV^2
SNO-NO	$m_{\text{lightest}} \ll \sqrt{\Delta m_{\text{sol}}^2} \ll \sqrt{\Delta m_{\text{atm}}^2}$	$\Delta m_{\text{sol}}^2 |U_{e2}|^2 + \Delta m_{\text{atm}}^2|U_{e3}|^2 + \Delta m_s^2|U_{e4}|^2$	Same as (I)	$\Delta m_s^2|U_{e4}|^2$
	$\sqrt{\Delta m_{\text{sol}}^2} \ll m_{\text{lightest}} \ll \sqrt{\Delta m_{\text{atm}}^2}$	$m_{\text{lightest}}^2\cdot$	Same as (I)	$\Delta m_s^2|U_{e4}|^2$
SNO-IO	$m_{\text{lightest}} \ll \sqrt{\Delta m_{\text{sol}}^2} \ll \sqrt{\Delta m_{\text{atm}}^2}$	Δm_{atm}^2	Δm_{atm}^2	$\Delta m_{\text{atm}}^2 + \Delta m_s^2|U_{e4}|^2$
	$\sqrt{\Delta m_{\text{atm}}^2} \lesssim m_{\text{lightest}}$	m_{lightest}^2	m_{lightest}^2	$m_{\text{lightest}}^2 + \Delta m_s^2|U_{e4}|^2$
	$\sqrt{\Delta m_{\text{atm}}^2} \ll m_s^2 \ll m_{\text{lightest}}$	m_{lightest}^2	m_{lightest}^2	m_3^2
SIO-NO	$m_{\text{lightest}} \ll \sqrt{\Delta m_{\text{sol}}^2} \ll \Delta m_s^2$	Δm_s^2	Δm_s^2	Δm_s^2
	$\sqrt{\Delta m_s^2} \ll m_{\text{lightest}}$	m_{lightest}^2	m_{lightest}^2	m_{lightest}^2
SIO-IO	$m_{\text{lightest}} \ll \sqrt{\Delta m_{\text{atm}}^2}$	Same as SNO-IO	Same as SIO-NO	Same as SIO-NO
	$m_s^2 \ll \sqrt{\Delta m_{\text{atm}}^2} \ll m_{\text{lightest}}$	m_{lightest}^2	N.A	N.A.
		N.A.	m_{lightest}	m_{lightest}

TABLE X. The table depicts expressions of $m_{\beta\beta}$ in third, fourth, and fifth columns corresponding to $\Delta m_s^2 = 10^{-4}$, 10^{-2}, and 1.3 eV^2, respectively, for various mass spectra given in the first column under different regions shown in column two.

Mass Spectra	Region	Expression of $m_{\beta\beta}$		
		(I) $\Delta m_s^2 = 10^{-4}$ eV^2	(II) $\Delta m_s^2 = 10^{-2}$ eV^2	(III) $\Delta m_s^2 = 1.3$ eV^2
SNO-NO	$m_1 \approx 0$	$\sqrt{\Delta m_{\text{sol}}^2}\,U_{e2}^2 e^{i\alpha} + \sqrt{\Delta m_{\text{atm}}^2}\,U_{e3}^2 e^{i\beta} + \sqrt{\Delta m_s^2}\,U_{e4}^2 e^{i\gamma}$	$\sqrt{\Delta m_{\text{sol}}^2}\,U_{e2}^2 e^{i\alpha} + \sqrt{\Delta m_{\text{atm}}^2}\,U_{e3}^2 e^{i\beta}$	Same as (I)
	$m_1 \approx m_2 \approx m_3$	N.A.	N.A.	Same as (II)
	$m_1 \approx m_2 \approx m_4$	$m_1[U_{e1}^2 + U_{e2}^2 e^{i\alpha} + U_{e4}^2 e^{i\gamma}]$	$m_1[U_{e1}^2 + U_{e2}^2 e^{i\alpha}]$	N.A.
	$m_1 \approx m_2 \approx m_3 \approx m_4$	$m_1[U_{e1}^2 + U_{e2}^2 e^{i\alpha} + U_{e4}^2 e^{i\gamma}]$	$m_1[U_{e1}^2 + U_{e2}^2 e^{i\alpha}]$	N.A.
SNO-IO	$m_3 \approx 0$	$\sqrt{\Delta m_{\text{atm}}^2}[U_{e1}^2 + U_{e2}^2 e^{i\alpha} + U_{e4}^2 e^{i\gamma}]$	$\sqrt{\Delta m_{\text{atm}}^2}[U_{e1}^2 + U_{e2}^2 e^{i\alpha}]$	$\sqrt{\Delta m_{\text{atm}}^2}[U_{e1}^2 + U_{e2}^2 e^{i\alpha}] + \sqrt{\Delta m_s^2}\,U_{e4}^2 e^{i\gamma}$
	$m_1 \approx m_2 \approx m_3$	$m_3[U_{e1}^2 + U_{e2}^2 e^{i\alpha} + U_{e4}^2 e^{i\gamma}]$	$m_3[U_{e1}^2 + U_{e2}^2 e^{i\alpha}]$	Same as (II)
	$m_1 \approx m_2 \approx m_3 \approx m_4$	$m_3[U_{e1}^2 + U_{e2}^2 e^{i\alpha} + U_{e4}^2 e^{i\gamma}]$	$m_3[U_{e1}^2 + U_{e2}^2 e^{i\alpha}]$	N.A.
SIO-NO	$m_4 \approx 0$	$\sqrt{\Delta m_s^2}[U_{e1}^2 + U_{e2}^2 e^{i\alpha}] + \sqrt{\Delta m_{\text{atm}}^2}\,U_{e3}^2 e^{i\beta}$	$\sqrt{\Delta m_s^2}[U_{e1}^2 + U_{e2}^2 e^{i\alpha}]$	Same as (II)
	$m_1 \approx m_2 \approx m_4$	$m_4[U_{e1}^2 + U_{e2}^2 e^{i\alpha} + U_{e4}^2 e^{i\gamma}]$	$m_4[U_{e1}^2 + U_{e2}^2 e^{i\alpha}]$	N.A.
	$m_1 \approx m_2 \approx m_3 \approx m_4$	$m_4[U_{e1}^2 + U_{e2}^2 e^{i\alpha} + U_{e4}^2 e^{i\gamma}]$	$m_4[U_{e1}^2 + U_{e2}^2 e^{i\alpha}]$	N.A.
SIO-IO	$m_{\text{lightest}} \approx 0$	$\sqrt{\Delta m_{\text{atm}}^2}[U_{e1}^2 + U_{e2}^2 e^{i\alpha} + U_{e4}^2 e^{i\gamma}]$	$\sqrt{\Delta m_s^2}[U_{e1}^2 + U_{e2}^2 e^{i\alpha}]$	Same as (II)
	$m_1 \approx m_2 \approx m_3 \approx m_4$	$m_3[U_{e1}^2 + U_{e2}^2 e^{i\alpha} + U_{e4}^2 e^{i\gamma}]$	$m_4[U_{e1}^2 + U_{e2}^2 e^{i\alpha}]$	N.A.

[1] Y. Fukuda *et al.*, Evidence for oscillation of atmospheric neutrinos, Phys. Rev. Lett. **81**, 1562 (1998).

[2] Q. R. Ahmad *et al.*, Direct evidence for neutrino flavor transformation from neutral current interactions in the Sudbury Neutrino Observatory, Phys. Rev. Lett. **89**, 011301 (2002).

[3] K. Eguchi *et al.*, First results from KamLAND: Evidence for reactor anti-neutrino disappearance, Phys. Rev. Lett. **90**, 021802 (2003).

[4] D. G. Michael *et al.*, Observation of muon neutrino disappearance with the MINOS detectors and the NuMI neutrino beam, Phys. Rev. Lett. **97**, 191801 (2006).

[5] Steven Weinberg, Baryon and lepton nonconserving processes, Phys. Rev. Lett. **43**, 1566 (1979).

[6] W. H. Furry, On transition probabilities in double beta-disintegration, Phys. Rev. **56**, 1184 (1939).

[7] Junpei Shirai, KamLAND-Zen experiment, *Proc. Sci.* HQL2018 (2018) 050.

[8] M. Agostini *et al.*, Final results of GERDA on the search for neutrinoless double-β decay, Phys. Rev. Lett. **125**, 252502 (2020).

[9] M. Aker *et al.*, Direct neutrino-mass measurement with sub-electronvolt sensitivity, Nat. Phys. **18**, 160 (2022).

[10] N. Aghanim *et al.*, Planck 2018 results. VI. Cosmological parameters, Astron. Astrophys. **641**, A6 (2020); **652**, C4(E) (2021).

[11] A. Aguilar *et al.*, Evidence for neutrino oscillations from the observation of $\bar{\nu}_e$ appearance in a $\bar{\nu}_\mu$ beam, Phys. Rev. D **64**, 112007 (2001).

[12] A. A. Aguilar-Arevalo *et al.*, Updated MiniBooNE neutrino oscillation results with increased data and new background studies, Phys. Rev. D **103**, 052002 (2021).

[13] W. Hampel *et al.*, Final results of the Cr-51 neutrino source experiments in GALLEX, Phys. Lett. B **420**, 114 (1998).

[14] Dzh. N. Abdurashitov *et al.*, The Russian-American gallium experiment (SAGE) Cr neutrino source measurement, Phys. Rev. Lett. **77**, 4708 (1996).

[15] V. V. Barinov *et al.*, Results from the Baksan Experiment on Sterile Transitions (BEST), Phys. Rev. Lett. **128**, 232501 (2022).

[16] Srubabati Goswami, Accelerator, reactor, solar and atmospheric neutrino oscillation: Beyond three generations, Phys. Rev. D **55**, 2931 (1997).

[17] P. Abratenko *et al.*, Search for an excess of electron neutrino interactions in MicroBooNE using multiple final-state topologies, Phys. Rev. Lett. **128**, 241801 (2022).

[18] P. Abratenko *et al.*, Search for an anomalous excess of charged-current quasielastic νe interactions with the Micro-BooNE experiment using deep-learning-based reconstruction, Phys. Rev. D **105**, 112003 (2022).

[19] P. Abratenko *et al.*, Search for an anomalous excess of charged-current νe interactions without pions in the final state with the MicroBooNE experiment, Phys. Rev. D **105**, 112004 (2022).

[20] P. Abratenko *et al.*, First constraints on light sterile neutrino oscillations from combined appearance and disappearance searches with the MicroBooNE detector, Phys. Rev. Lett. **130**, 011801 (2023).

[21] Peter B. Denton, Sterile neutrino search with Micro-BooNE's electron neutrino disappearance data, Phys. Rev. Lett. **129**, 061801 (2022).

[22] A. A. Aguilar-Arevalo *et al.*, MiniBooNE and MicroBooNE combined fit to a $3 + 1$ sterile neutrino scenario, Phys. Rev. Lett. **129**, 201801 (2022).

[23] P. C. de Holanda and A. Yu. Smirnov, Solar neutrino spectrum, sterile neutrinos and additional radiation in the Universe, Phys. Rev. D **83**, 113011 (2011).

[24] André de Gouvêa, Giancarlo Jusino Sánchez, and Kevin J. Kelly, Very light sterile neutrinos at NOvA and T2K, Phys. Rev. D **106**, 055025 (2022).

[25] Sanjib Kumar Agarwalla, Sabya Sachi Chatterjee, and Antonio Palazzo, Physics potential of ESSνSB in the presence of a light sterile neutrino, J. High Energy Phys. 12 (2019) 174.

[26] Sanjib Kumar Agarwalla, Sabya Sachi Chatterjee, and Antonio Palazzo, Signatures of a light sterile neutrino in T2HK, J. High Energy Phys. 04 (2018) 091.

[27] Animesh Chatterjee, Srubabati Goswami, and Supriya Pan, Probing mass orderings in presence of a very light sterile neutrino in a liquid argon detector, Nucl. Phys. **B996**, 116370 (2023).

[28] Animesh Chatterjee, Srubabati Goswami, and Supriya Pan, Matter effect in presence of a sterile neutrino and resolution of the octant degeneracy using a liquid argon detector, Phys. Rev. D **108**, 095050 (2023).

[29] Srubabati Goswami and Werner Rodejohann, Constraining mass spectra with sterile neutrinos from neutrinoless double beta decay, tritium beta decay and cosmology, Phys. Rev. D **73**, 113003 (2006).

[30] A. Ashtari Esfahani *et al.*, The Project 8 neutrino mass experiment, in *Snowmass 2021* (2022), p. 3, arXiv:2203.07349.

[31] G. Adhikari *et al.*, nEXO: Neutrinoless double beta decay search beyond 10^{28} year half-life sensitivity, J. Phys. G **49**, 015104 (2022).

[32] Ziro Maki, Masami Nakagawa, and Shoichi Sakata, Remarks on the unified model of elementary particles, Prog. Theor. Phys. **28**, 870 (1962).

[33] Ivan Esteban, M. C. Gonzalez-Garcia, Michele Maltoni, Thomas Schwetz, and Albert Zhou, The fate of hints: Updated global analysis of three-flavor neutrino oscillations, J. High Energy Phys. 09 (2020) 178.

[34] P. Adamson *et al.*, Search for sterile neutrinos in MINOS and MINOS + using a two-detector fit, Phys. Rev. Lett. **122**, 091803 (2019).

[35] M. A. Acero *et al.*, White paper on light sterile neutrino searches and related phenomenology, arXiv:2203.07323.

[36] Jack J. Bennett, Gilles Buldgen, Pablo F. De Salas, Marco Drewes, Stefano Gariazzo, Sergio Pastor, and Yvonne Y. Y. Wong, Towards a precision calculation of N_{eff} in the Standard Model II: Neutrino decoupling in the presence of flavour oscillations and finite-temperature QED, J. Cosmol. Astropart. Phys. 04 (2021) 073.

[37] Kensuke Akita and Masahide Yamaguchi, A precision calculation of relic neutrino decoupling, J. Cosmol. Astropart. Phys. 08 (2020) 012.

[38] Julien Froustey, Cyril Pitrou, and Maria Cristina Volpe, Neutrino decoupling including flavour oscillations and

primordial nucleosynthesis, J. Cosmol. Astropart. Phys. 12 (2020) 015.

[39] Carlos E. Yaguna, Sterile neutrino production in models with low reheating temperatures, J. High Energy Phys. 06 (2007) 002.

[40] Kevork N. Abazajian, Sterile neutrinos in cosmology, Phys. Rep. **711**–**712**, 1 (2017).

[41] Basudeb Dasgupta and Joachim Kopp, Cosmologically Safe eV-scale sterile neutrinos and improved dark matter structure, Phys. Rev. Lett. **112**, 031803 (2014).

[42] Xiaoyong Chu, Basudeb Dasgupta, and Joachim Kopp, Sterile neutrinos with secret interactions—lasting friendship with cosmology, J. Cosmol. Astropart. Phys. 10 (2015) 011.

[43] Adam G. Riess *et al.*, New parallaxes of galactic cepheids from spatially scanning the Hubble Space Telescope: Implications for the Hubble constant, Astrophys. J. **855**, 136 (2018).

[44] D. M. Scolnic *et al.*, The complete light-curve sample of spectroscopically confirmed SNe Ia from Pan-STARRS1 and cosmological constraints from the Combined Pantheon Sample, Astrophys. J. **859**, 101 (2018).

[45] Steffen Hagstotz, Pablo F. de Salas, Stefano Gariazzo, Martina Gerbino, Massimiliano Lattanzi, Sunny Vagnozzi, Katherine Freese, and Sergio Pastor, Bounds on light sterile neutrino mass and mixing from cosmology and laboratory searches, Phys. Rev. D **104**, 123524 (2021).

[46] Ninetta Saviano, Alessandro Mirizzi, Ofelia Pisanti, Pasquale Dario Serpico, Gianpiero Mangano, and Gennaro Miele, Multi-momentum and multi-flavour active-sterile neutrino oscillations in the early universe: Role of neutrino asymmetries and effects on nucleosynthesis, Phys. Rev. D **87**, 073006 (2013).

[47] Robert Foot and R. R. Volkas, Reconciling sterile neutrinos with big bang nucleosynthesis, Phys. Rev. Lett. **75**, 4350 (1995).

[48] Kevork Abazajian, Nicole F. Bell, George M. Fuller, and Yvonne Y. Y. Wong, Cosmological lepton asymmetry, primordial nucleosynthesis, and sterile neutrinos, Phys. Rev. D **72**, 063004 (2005).

[49] Alessandro Mirizzi, Ninetta Saviano, Gennaro Miele, and Pasquale Dario Serpico, Light sterile neutrino production in the early universe with dynamical neutrino asymmetries, Phys. Rev. D **86**, 053009 (2012).

[50] Steen Hannestad, Rasmus Sloth Hansen, and Thomas Tram, How self-interactions can reconcile sterile neutrinos with cosmology, Phys. Rev. Lett. **112**, 031802 (2014).

[51] James M. Cline, Viable secret neutrino interactions with ultralight dark matter, Phys. Lett. B **802**, 135182 (2020).

[52] Yasaman Farzan, Ultra-light scalar saving the $3 + 1$ neutrino scheme from the cosmological bounds, Phys. Lett. B **797**, 134911 (2019).

[53] Francesco Forastieri, Massimiliano Lattanzi, Gianpiero Mangano, Alessandro Mirizzi, Paolo Natoli, and Ninetta Saviano, Cosmic microwave background constraints on secret interactions among sterile neutrinos, J. Cosmol. Astropart. Phys. 07 (2017) 038.

[54] Graciela B. Gelmini, Philip Lu, and Volodymyr Takhistov, Cosmological dependence of non-resonantly produced sterile neutrinos, J. Cosmol. Astropart. Phys. 12 (2019) 047.

[55] Graciela B. Gelmini, Philip Lu, and Volodymyr Takhistov, Visible sterile neutrinos as the earliest relic probes of cosmology, Phys. Lett. B **800**, 135113 (2020).

[56] Takuya Hasegawa, Nagisa Hiroshima, Kazunori Kohri, Rasmus S. L. Hansen, Thomas Tram, and Steen Hannestad, MeV-scale reheating temperature and cosmological production of light sterile neutrinos, J. Cosmol. Astropart. Phys. 08 (2020) 015.

[57] Hooman Davoudiasl and Peter B. Denton, Sterile neutrino shape shifting caused by dark matter, Phys. Rev. D **108**, 035013 (2023).

[58] Vincenzo Cirigliano, Wouter Dekens, Jordy De Vries, Michael L. Graesser, Emanuele Mereghetti, Saori Pastore, and Ubirajara Van Kolck, New leading contribution to neutrinoless double-β decay, Phys. Rev. Lett. **120**, 202001 (2018).

[59] V. Cirigliano, W. Dekens, J. De Vries, M. L. Graesser, E. Mereghetti, S. Pastore, M. Piarulli, U. Van Kolck, and R. B. Wiringa, Renormalized approach to neutrinoless double-β decay, Phys. Rev. C **100**, 055504 (2019).

[60] Oliver Scholer, Jordy de Vries, and Lukáš Gráf, νDoBe—A Python tool for neutrinoless double beta decay, J. High Energy Phys. 08 (2023) 043.

[61] G. L. Fogli, E. Lisi, A. Marrone, A. Melchiorri, A. Palazzo, P. Serra, and J. Silk, Observables sensitive to absolute neutrino masses: Constraints and correlations from world neutrino data, Phys. Rev. D **70**, 113003 (2004).